PHYSICAL REVIEW D **91,** 115007 (2015)

Nambu-Goldstone dark matter in a scale invariant bright hidden sector

Yoshitaka Ametani,[*] Mayumi Aoki,[†] Hiromitsu Goto,[‡] and Jisuke Kubo[§]

Institute for Theoretical Physics, Kanazawa University, Kanazawa 920-1192, Japan

(Received 11 May 2015; published 8 June 2015)

We consider a scale invariant extension of the standard model (SM) with a combined breaking of conformal and electroweak symmetry in a strongly interacting hidden $SU(n_c)$ gauge sector with n_f vector-like hidden fermions. The (pseudo) Nambu-Goldstone bosons that arise due to dynamical chiral symmetry breaking are dark matter (DM) candidates. We focus on $n_f = n_c = 3$, where $SU(3)$ is the largest symmetry group of hidden flavor which can be explicitly broken into either $U(1) \times U(1)$ or $SU(2) \times U(1)$. We study DM properties and discuss consistent parameter space for each case. Because of different mechanisms of DM annihilation the consistent parameter space in the case of $SU(2) \times U(1)$ is significantly different from that of $SU(3)$ if the hidden fermions have a SM $U(1)_Y$ charge of $O(1)$.

DOI: 10.1103/PhysRevD.91.115007 PACS numbers: 95.35.+d, 12.60.-i

I. INTRODUCTION

What is the origin of mass? This is a long-standing question and still remains unsolved [1].

The recent discovery of the Higgs particle [2,3] may hint how to go beyond the standard model (SM). The measured Higgs mass and top quark mass [4] are such that the SM remains perturbative below the Planck scale [5–7]. According to Bardeen [8], "the SM does not, by itself, have a fine-tuning problem." Because the Higgs mass term is the only term, which breaks scale invariance at the Lagrangian level in the SM, we may ask about the origin of this mass term. Mostly scale invariance is hardly broken by quantum anomaly [9]. Therefore, a dimensional transmutation can occur at the quantum level, which can be used to generate a la Coleman-Weinberg [10] the Higgs mass term in a classically scale invariant extension of the SM [11–45]. Dynamical chiral symmetry breaking [46,47] can also be used [48–54]. The idea is the same as that of technicolor model [55,56], where the only difference is that we now allow the existence of fundamental scalars.

In this paper we consider the latter possibility, in particular the model studied in [48–52]. In this model the scale, generated in a QCD-like hidden sector, is transmitted to the SM sector via a real SM singlet scalar S to trigger spontaneous breaking of electroweak (EW) gauge symmetry [48,49] (see also [57]). Moreover, due to the dynamical chiral symmetry breaking in the hidden sector there exist Nambu-Goldstone (NG) bosons, which are massive, because the coupling y of S with the hidden sector fermions breaks explicitly chiral symmetry. Therefore, the mass scale of the NG bosons, which are dark matter (DM) candidates, is not independent (as it is not the case in the most of DM models); it is smaller than the hidden sector scale, which is in the TeV region unless the coupling y is very small, i.e., $\lesssim O(10^{-4})$.

As in [51,52] we employ the Nambu-Jona-Lasinio (NJL) theory [46,47] as a low-energy effective theory of the hidden sector and base our calculations on the self-consistent mean field (SCMF) approximation [58,59] of the NJL theory, which is briefly outlined in Sec. III. In [51,52] the maximal global flavor symmetry $SU(3)_V$ [along with a $U(1)_V$] has been assumed. In this paper we relax this assumption and consider in detail the cases, in which $SU(3)_V$ is broken into its subgroups. We find in Sec. IV that the consistent parameter space can be considerably extended if $SU(3)_V$ is broken to its subgroup $SU(2)_V \times U(1)_{\tilde{B}'}$. The main reason is that, if $SU(3)_V$ is broken, a new mechanism for the DM annihilation, inverse DM conversion, becomes operative at finite temperature: A pair of lighter DM particles annihilate into a pair of heavier (would-be) DM particles, which subsequently decay into SM particles (mainly into two γs).

Before we discuss the DM phenomenology of the model, we develop an effective theory for DM interactions (a linear sigma model) in the framework of the SCMF approximation of the NJL theory. Using the effective theory we compute the DM relic abundance and analyze the direct and indirect DM detection possibilities in Sec. IV. Section V is devoted to Conclusion, and in Appendix A we give explicitly the NJL Lagrangian in the SCMF approximation in the case that $SU(3)_V$ is broken into $U(1)_{\tilde{B}'} \times U(1)_{\tilde{B}}$. In Appendix B the inverse DM (mesons for QCD) propagators and also how the NJL parameters are fixed can be found. The one-loop integrals that are used in our calculations are collected in Appendix C.

II. THE MODEL

We consider a classically scale invariant extension of the SM studied in [48–52][1] which consists of a hidden

[*]ametani@hep.s.kanazawa-u.ac.jp
[†]mayumi@hep.s.kanazawa-u.ac.jp
[‡]goto@hep.s.kanazawa-u.ac.jp
[§]jik@hep.s.kanazawa-u.ac.jp

[1]See also [60].

$SU(n_c)_H$ gauge sector coupled via a real singlet scalar S to the SM. The hidden sector Lagrangian of the model is written as

$$\mathcal{L}_{\rm H} = -\frac{1}{2}{\rm Tr}F^2 + {\rm Tr}\bar{\psi}(i\gamma^\mu\partial_\mu + g_H\gamma^\mu G_\mu + g'Q\gamma^\mu B_\mu - yS)\psi, \quad (1)$$

where G_μ is the gauge field for the hidden QCD, B_μ is the $U(1)_Y$ gauge field, i.e.,

$$B_\mu = \cos\theta_W A_\mu - \sin\theta_W Z_\mu, \qquad g' = e/\cos\theta_W, \quad (2)$$

and the n_f (Dirac) fermions $\psi_i (i = 1, \ldots, n_f)$ in the hidden sector belong to the fundamental representation of $SU(n_c)_H$. The trace in (1) is taken over the flavor as well as the color indices. The hidden fermions carry a common $U(1)_Y$ charge Q, implying that they contribute only to Π_{YY} of the gauge boson self-energy diagrams so that the S, T, U parameters remain unchanged. The $\mathcal{L}_{\rm SM+S}$ part of the total Lagrangian $\mathcal{L}_T = \mathcal{L}_{\rm H} + \mathcal{L}_{\rm SM+S}$ contains the SM gauge and Yukawa interactions along with the scalar potential

$$V_{\rm SM+S} = \lambda_H(H^\dagger H)^2 + \frac{1}{4}\lambda_S S^4 - \frac{1}{2}\lambda_{HS}S^2(H^\dagger H), \quad (3)$$

where $H^T = (H^+, (h + iG)\sqrt{2})$ is the SM Higgs doublet field, with H^+ and G as the would-be Nambu-Goldstone fields.[2] The basic mechanism to trigger the EW symmetry breaking is very simple: The nonperturbative effect of dynamical chiral symmetry breaking in the hidden sector generates a robust scale which is transferred into the SM sector through the real singlet S. Then the mass term for the Higgs potential is generated via the Higgs portal term in (3), where the "−" in front of the positive λ_{HS} is an assumption.

A. Global symmetries

The Yukawa coupling of the hidden fermions with the singlet S breaks explicitly chiral symmetry. Therefore, in the limit of the vanishing Yukawa coupling matrix y_{ij} the global symmetry $SU(n_f)_L \times SU(n_f)_R \times U(1)_V \times U(1)_A$ is present at the classical level, where $U(1)_A$ is broken by anomaly at the quantum level down to its discrete subgroup Z_{2n_f}, and the unbroken $U(1)_V$ ensures the conservation of the hidden baryon number. The non-Abelian part of the chiral symmetry $SU(n_f)_L \times SU(n_f)_R$ is broken dynamically down to its diagonal subgroup $SU(n_f)_V$ by the nonvanishing chiral condensates $\langle\bar{\psi}_i\psi_i\rangle$, implying the existence of $n_f^2 - 1$ NG bosons $\phi_a (a = 1, \ldots, n_f^2 - 1)$. In the $n_f = 3$ case the NG bosons are like the mesons in the real hadron world:

$$\tilde{\pi}^0 = \phi_3, \qquad \tilde{\pi}^\pm = (\phi_1 \mp i\phi_2)/\sqrt{2},$$
$$\tilde{K}^\pm = (\phi_4 \mp i\phi_5)/\sqrt{2}, \qquad \tilde{K}^0(\tilde{\bar{K}}^0) = (\phi_6 + (-)i\phi_7)/\sqrt{2},$$
$$\tilde{\eta}^8 = \phi_8, \quad (4)$$

where $\tilde{\eta}^8$ will mix with $\tilde{\eta}^0$ to form the mass eigenstates $\tilde{\eta}$ and $\tilde{\eta}'$. (The ˜ should avoid the confusion with the real mesons π^0 etc.)

In the presence of the Yukawa coupling the chiral symmetry is explicitly broken; this is the only coupling which breaks the chiral symmetry explicitly. Because of this coupling the NG bosons become massive. An appropriate chiral rotation of ψ_i can diagonalize the Yukawa coupling matrix:

$$y_{ij} = y_i\delta_{ij}(y_i \geq 0) \quad (5)$$

can be assumed without loss of generality, which implies that $U(1)^{n_f-1}$ corresponding to the elements of the Cartan subalgebra of $SU(n_f)$ are unbroken. We assume that none of y_i vanishes so that all the NG bosons are massive. If two y_is are the same, say $y_1 = y_2$, one $U(1)$ is promoted to an $SU(2)$. Similarly, if three y_is are the same, a product group $U(1)\times U(1)$ is promoted to an $SU(3)$, and so on. In addition to these symmetry groups, there exists a discrete Z_4,

$$Z_4: \psi_i \to (\exp i(\pi/2)\gamma_5)\psi_i = i\gamma_5\psi_i \quad \text{and} \quad S \to -S. \quad (6)$$

This discrete symmetry is anomalous for odd n_f, because the chiral transformation in (6) is an element of the anomalous $U(1)_A$. If n_f is even, then the chiral transformation is an element of the anomaly-free subgroup Z_{2n_f} of $U(1)_A$. Needless to say that this Z_4 is broken by a nonvanishing vacuum expectation value (VEV) of S, which is essential to trigger the EW gauge symmetry breaking.

B. Dark matter candidates

The NG bosons, which arise due to the dynamical chiral symmetry breaking in the hidden sector, are good DM candidates, because they are neutral and their interactions with the SM part start to exist at the one-loop level so that they are weak. However, not all NG bosons can be DM, because their stability depends on the global symmetries that are intact. In the following we consider the case for $n_f = 3$, which can be simply extended to an arbitrary n_f. For $n_f = 3$ there are three possibilities of the global symmetries:

$$\text{(i)}\ U(1)_{\tilde{B}'} \times U(1)_{\tilde{B}} \quad \text{if } y_1 \neq y_2 \neq y_3, \quad (7)$$

$$\text{(ii)}\ SU(2)_V \times U(1)_{\tilde{B}} \quad \text{if } y_1 = y_2 \neq y_3, \quad (8)$$

[2]This classically scale invariant model is perturbatively renormalizable, and the Green's functions are infrared finite [61,62].

TABLE I. The NG bosons and DM candidates for $n_f = 3$.

	$\tilde{\pi}^0$	$\tilde{\pi}^+$	$\tilde{\pi}^-$	$\tilde{K}^0$	$\tilde{K}^+$	$\tilde{K}^-$	$\tilde{\bar{K}}^0$	$\tilde{\eta}^8$
$U(1)_Y$ charge	0	0	0	0	0	0	0	0
$\tilde{B}'$	0	2	−2	−1	1	−1	1	0
$\tilde{B}$	0	0	0	3	3	−3	−3	0
$SU(2)_V$		**3**		**2**		**2**		**1**
$SU(3)_V$					**8**			

$$\text{(iii) } SU(3)_V \quad \text{if } y_1 = y_2 = y_3, \tag{9}$$

where we have suppressed $U(1)_V$ which always exists, and the case (iii) has been treated in detail in [52]. Without loss of generality we can assume that the elements of the Cartan subalgebra corresponding to $U(1)_{\tilde{B}'}$ and $U(1)_{\tilde{B}}$ are

$$\tilde{B}' = \begin{pmatrix} 1 & 0 & 0 \\ 0 & -1 & 0 \\ 0 & 0 & 0 \end{pmatrix}, \qquad \tilde{B} = \begin{pmatrix} 1 & 0 & 0 \\ 0 & 1 & 0 \\ 0 & 0 & -2 \end{pmatrix}. \tag{10}$$

In Table I we show the NG bosons for $n_f = 3$ with their quantum numbers. As we can see from Table I the NG bosons $\tilde{\pi}^0$ and $\tilde{\eta}^8$ are unstable for the case (i) and in fact can decay into two γs, while for the case (ii) only $\tilde{\eta}^8$ is unstable. Whether the stable NG bosons can be realistic DM particles is a dynamical question, which we will address later on.

C. Perturbativity and stability of the scalar potential at high energy

Before we discuss the nonperturbative effects, we consider briefly the perturbative part at high energies, i.e., above the scale of the dynamical chiral symmetry breaking in the hidden sector. As explained in the Introduction, it is essential for our scenario of explaining the origin of the EW scale to work that the scaler potential is unbounded below and the theory remains perturbative (no Landau pole) below the Planck scale. So, we require:

$$4\pi > \lambda_H, \quad \lambda_S > 0, \quad 4\pi > \lambda_{HS} > 0, \quad |y|^2 < 4\pi, \tag{11}$$

$$2\sqrt{\lambda_H \lambda_S} - \lambda_{HS} > 0. \tag{12}$$

In the following discussion we assume that the perturbative regime (of the hidden sector) starts around $q_0 = 1$ TeV and $g_H^2(q_0)/4\pi \simeq 1$. Although in this model the Higgs mass depends mainly on two parameters, λ_H and λ_{HS}, lowering $\lambda_H(q_0) < 0.13$ will destabilize the Higgs potential while increasing $\lambda_H(q_0) > 0.14$ will require a larger mixing with S, which is strongly constrained. Therefore, we consider the RG running of the couplings with $\lambda_H(q_0)$ fixed at 0.135 and rely on one-loop approximations. In the case that the hypercharge Q of the hidden fermions is different from zero, these fermions contribute to the renormalization group (RG) running of the $U(1)_Y$ gauge coupling considerably. We found that $Q \lesssim 0.8$ should be satisfied for g' to remain perturbative below the Planck scale.

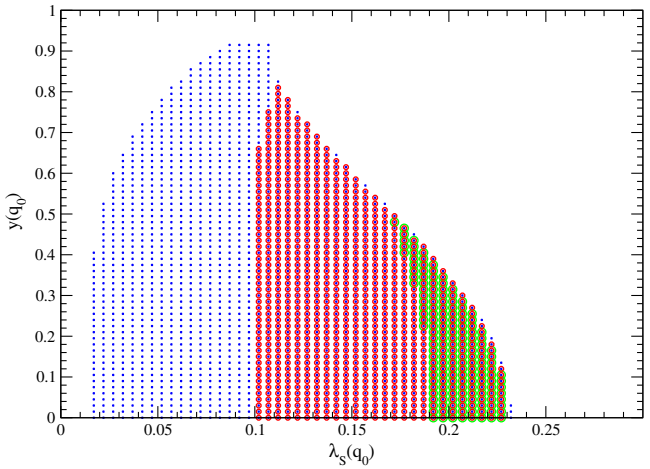

FIG. 1 (color online). Stability constraint. The allowed area in the $\lambda_S - y$ plane for different values of $\lambda_{HS}(q_0)$ with $\lambda_H(q_0)$ fixed at 0.135 ($q_0 = 1$ TeV) is shown, where we have used $Q = 1/3$ and assumed the $SU(3)_V$ flavor symmetry defined in (9). The green (dark gray) circles, red (gray) circles, and blue (light gray) points stand for $\lambda_{HS}(q_0) = 0.1, 0.06$, and 0.02.

Because of (12) the range of λ_S is constrained for a given λ_{HS} and λ_H: The larger λ_{HS} is, the larger λ_S has to be. But there is an upper limit for $\lambda_S(q_0)$ because of perturbativity. In Fig. 1 we show the allowed area in the $\lambda_S - y$ plane for different values of $\lambda_{HS}(q_0)$ with $\lambda_H(q_0)$ fixed at 0.135 in the $SU(3)_V$ case (9), i.e., $y = y_1 = y_2 = y_3$.[3] The green (dark gray) circles, red (gray) circles, and blue (light gray) points stand for $\lambda_{HS}(q_0) = 0.1, 0.06$, and 0.02. There will be no allowed region for $\lambda_{HS}(q_0) \gtrsim 0.12$. We have used $Q = 1/3$, but the allowed area does not depend very much on Q as long as $Q < 0.8$ is satisfied [which ensures perturbativity of the $U(1)_Y$ gauge coupling]. If $SU(3)_V$ is broken, then the vertical axis in Fig. 1 represents the largest among y_is.

III. NAMBU-JONA-LASINIO METHOD

A. NJL Lagrangian in a mean-field approximation

Following [51] we replace the high energy Lagrangian $\mathcal{L}_H$ in (1) by the NJL Lagrangian

$$\mathcal{L}_{\text{NJL}} = \text{Tr}\bar{\psi}(i\gamma^\mu \partial_\mu + g' Q \gamma^\mu B_\mu - yS)\psi + 2G\text{Tr}\Phi^\dagger \Phi + G_D(\det \Phi + \text{H.c.}), \tag{13}$$

where

[3]The same analysis has been performed in [52], but without including the constraint (12).

$$\Phi_{ij} = \bar{\psi}_i(1-\gamma_5)\psi_j = \frac{1}{2}\sum_{a=0}^{n_f^2-1} \lambda^a_{ji}\mathrm{Tr}\bar{\psi}\lambda^a(1-\gamma_5)\psi, \quad (14)$$

and $\lambda^a (a = 1, \ldots, n_f^2 - 1)$ are the Gell-Mann matrices with $\lambda^0 = \sqrt{2/3}\mathbf{1}$. The effective Lagrangian $\mathcal{L}_{\mathrm{NJL}}$ has three-dimensional parameters G, G_D and the cutoff Λ, which have canonical dimensions of -2, -5, and 1, respectively. Since the original Lagrangian $\mathcal{L}_H$ has only one independent scale, the parameters G, G_D, and Λ are not independent. We restrict ourselves to $n_c = n_f = 3$, because in this case these parameters, up-to an overall scale, can be approximately fixed from hadron physics [58,59]. The six-fermi interaction in (13) is present due to chiral anomaly of the axial $U(1)_A$ and is invariant under Z_6, so that the NJL Lagrangian (13) has the same global symmetry as the high energy Lagrangian (1). Furthermore, as we mentioned in Sec. II A, we can assume without loss of generality that the Yukawa coupling matrix y is diagonal [see (5)]. To deal with the nonrenormalizable Lagrangian (13) we employ [51] the SCMF approximation which has been intensely studied by Hatsuda and Kunihiro [58,59] for hadron physics. The NJL parameters for the hidden QCD is then obtained by the upscaling of the actual values of G, G_D and the cutoff Λ from QCD hadron physics. That is, we assume that the dimensionless combinations

$$G^{1/2}\Lambda = 1.82, \qquad (-G_D)^{1/5}\Lambda = 2.29, \quad (15)$$

which are satisfied for hadrons, remain unchanged for a higher scale of Λ.

Below we briefly outline the SCMF approximation. We go via a Bogoliubov-Valatin transformation from the perturbative vacuum to the "BCS" vacuum, which we simply denote by $|0\rangle$. This vacuum is so defined that the mesons (mean fields) are collected in the VEV of the chiral bilinear:

$$\varphi \equiv \langle 0|\bar{\psi}(1-\gamma_5)\psi|0\rangle = -\frac{1}{4G}(\mathrm{diag}(\tilde{\sigma}_1, \tilde{\sigma}_2, \tilde{\sigma}_3) + i(\lambda^a)^T\phi_a), \quad (16)$$

where we denote the pseudo-NG boson fields after spontaneous chiral symmetry breaking by ϕ_a. The dynamics of the hidden sector creates a nonvanishing chiral condensate $\langle 0|\bar{\psi}_i\psi_i|0\rangle$ which is nothing but $-\langle\tilde{\sigma}_i\rangle/4G$. The actual value of $\langle\tilde{\sigma}_i\rangle$ can be obtained through the minimization of the scalar potential, as we describe shortly. In the SCMF approximation one splits up the NJL Lagrangian (13) into the sum

$$\mathcal{L}_{\mathrm{NJL}} = \mathcal{L}_0 + \mathcal{L}_I, \quad (17)$$

where $\mathcal{L}_I$ is normal ordered (i.e., $\langle 0|\mathcal{L}_I|0\rangle = 0$), and $\mathcal{L}_0$ contains at most fermion bilinears which are not normal ordered. At the nontrivial lowest order only $\mathcal{L}_0$ is relevant for the calculation of the effective potential, the DM mass, and the DM interactions. The explicit form for $\mathcal{L}_0$ can be found in Appendix A. The effective potential can be obtained by integrating out the hidden fermion fields in the BCS vacuum. At the one-loop level we find

$$V_{\mathrm{NJL}}(\tilde{\sigma}_i, S) = \frac{1}{8G}\sum_{i=1,2,3}\tilde{\sigma}_i^2 - \frac{G_D}{16G^3}\tilde{\sigma}_1\tilde{\sigma}_2\tilde{\sigma}_3 - \sum_{i=1,2,3} n_c I_V(M_i), \quad (18)$$

where $I_V(m)$ is given in Eq. (C1), and the constituent fermion masses M_i are given by

$$M_i = \tilde{\sigma}_i + y_i S - \frac{G_D}{8G^2}\tilde{\sigma}_{i+1}\tilde{\sigma}_{j+2}, \quad (19)$$

where $\tilde{\sigma}_4 = \tilde{\sigma}_1$ and $\tilde{\sigma}_5 = \tilde{\sigma}_2$. Once the free parameters of the model $y_i, \lambda_H, \lambda_{HS}, \lambda_S$ are given, the VEVs of $\tilde{\sigma}_i$ and S can be determined through the minimization of the scalar potential $V_{\mathrm{SM+S}} + V_{\mathrm{NJL}}$, where $V_{\mathrm{SM+S}}$ is defined in (3). After the minimum of the scalar potential is fixed, the mass spectrum for the CP-even particles h, S, and $\tilde{\sigma}$ as well as the DM candidates with their properties are obtained.

B. The value of y and hidden chiral phase transition

The Yukawa coupling in (1) violates explicitly chiral symmetry and plays a similar role as the current quark mass in QCD. It is well known that the nature of chiral phase transition in QCD depends on the value of the current quark mass. Therefore, it is expected that the value of y strongly influences the nature of the chiral phase transition in the hidden sector, which has been confirmed in [51]. The hidden chiral phase transition occurs above the EW phase transition, where the nature of the EW phase transition is not known yet. In the following discussions, we restrict ourselves to

$$0 < y \lesssim 0.006, \quad (20)$$

because in this case the hidden chiral phase transition is a strong first order transition [51] and can produce gravitational wave back ground [63,64], which could be observed by future experiments such as Evolved Laser Interferometer Space Antenna (eLISA) experiment [65]. Needless to say that the smaller is y, the better is the NJL approximation to chiral symmetry breaking.

IV. DARK MATTER PHENOMENOLOGY

A. Dark matter masses

Our DM candidates are the pseudo-NG bosons, which occur due to the dynamical chiral symmetry breaking in the hidden sector. They are CP-odd scalars, and their masses

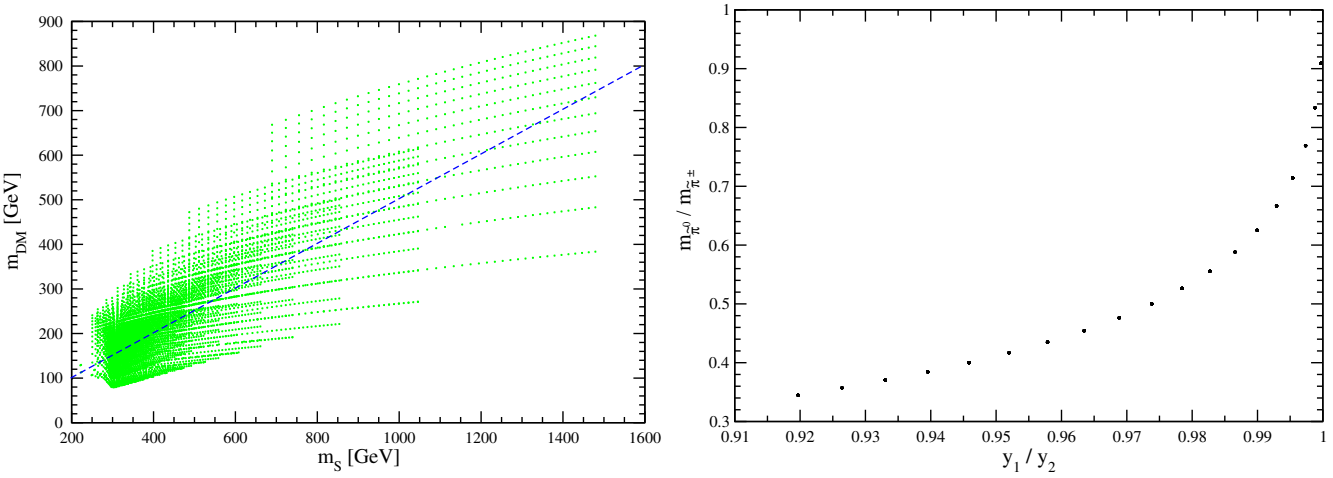

FIG. 2 (color online). Left: The area in the m_S-$m_{\rm DM}$ plane for $0.0005 < y_1 = y_2 = y_3 < 0.006$ in the $SU(3)_V$ case (9), where $m_{\rm DM} = m_{\tilde{\pi}^0} = m_{\tilde{\pi}^\pm} = m_{\tilde{K}^0} = m_{\tilde{K}^\pm} = m_{\tilde{\eta}}$. The ratio $m_S/m_{\rm DM} = 2$ is satisfied on the blue (gray) dashed line, on which the resonance condition in the s-channel diagram for the DM annihilation (Fig. 10) is satisfied. Right: The ratio $m_{\tilde{\pi}^0}/m_{\tilde{\pi}^\pm}$ versus y_1/y_2 in the $U(1)_{\tilde{B}'} \times U(1)_{\tilde{B}}$ case (7), where y_1 and y_3 are fixed at 0.002 and 0.006, respectively. The constraints imposed on λ_H, λ_{HS}, and λ_S are such that we obtain a correct Higgs mass and the perturbativity (11) as well as stability (12) constraints are satisfied.

are generated at one-loop in the SCMF approximation as the real meson masses, where we here, too, restrict ourselves to $n_c = n_f = 3$. Therefore, their inverse propagators can be calculated in a similar way as in the QCD case, which is given in Appendix B.

First we consider the $SU(3)_V$ case (9) to obtain the DM mass $m_{\rm DM}$[4] and the mass of the singlet m_S for $0.001 \lesssim y_1 = y_2 = y_3 \lesssim 0.006$. In Fig. 2 (left) we show the area in the m_S-$m_{\rm DM}$ plane, in which we obtain a correct Higgs mass, while imposing the perturbativity (11) as well as stability (12) constraints. The upper limit of $m_{\rm DM}$ for a given m_S is due to the upper limit of the Yukawa coupling [see (20)], while its lower limit comes from the lower limit of the Yukawa coupling, which is taken to be 0.0005 here. The upper limit for m_S is dictated by the upper limit of λ_S, which is fixed by the perturbativity and stability constraints (11) and (12). The lowest value of m_S, 250 GeV, comes from the lowest value of λ_S, which is set at 0.05 here. If $SU(3)_V$ is only slightly broken, the DM mass will not change very much.

We next consider the $U(1)_{\tilde{B}'} \times U(1)_{\tilde{B}}$ case (7). We may assume without loss of generality that the hierarchy $y_1 < y_2 < y_3$ is satisfied. In Fig. 2 (right) we show the ratio $m_{\tilde{\pi}^0}/m_{\tilde{\pi}^\pm}$ versus y_1/y_2, where we have fixed y_1 and y_3 at 0.002 and 0.006, respectively. We can conclude from Fig. 2 (right) that $\tilde{\pi}^0$ is the lightest among the pseudo-NG bosons and the ratio $m_{\tilde{\pi}^0}/m_{\tilde{\pi}^\pm}$ does not practically depend on the scalar couplings λ_H, λ_{HS}, and λ_S. The $SU(2)_V$ case (8) can be realized if two of y_i are the same. There are two independent possibilities: (a) $y_1 = y_2 < y_3$, and (b) $y_1 < y_2 = y_3$. The mass spectrum for the case (b) is similar to that for the $U(1)_{\tilde{B}'} \times U(1)_{\tilde{B}}$ case. In particular, $\tilde{\pi}^0$ is the lightest among the pseudo-NG bosons. As for the case (a) the mass hierarchy

$$m_{\tilde{\pi}} = m_{\tilde{\pi}^0} = m_{\tilde{\pi}^\pm} < m_{\tilde{K}} = m_{\tilde{K}^0} = m_{\tilde{K}^\pm} < m_{\tilde{\eta}} \qquad (21)$$

is always satisfied.

The different type of the DM mass spectrum will have an important consequence when discussing the DM relic abundance.

B. Effective interactions for DM decay and annihilations

As discussed in Sec. II B, if the $SU(3)_V$ flavor symmetry is broken to $U(1)_{\tilde{B}'} \times U(1)_{\tilde{B}}$, there will be two real decaying would-be DM particles $\tilde{\eta}, \tilde{\pi}^0$, and three pairs of complex DM particles $(\tilde{K}^0, \tilde{\bar{K}}^0)$, $\tilde{K}^\pm$, and $\tilde{\pi}^\pm$. Here we will derive effective interactions for these DM fields by integrating out the hidden fermions at the one-loop order. The one-loop integrals and their lowest order expressions of expansion in the external momenta in the large Λ limit are given in Appendix B. Except for the ϕ-ϕ-γ and ϕ-γ-γ interactions, we assume $SU(2)_V$ flavor symmetry, i.e.,

$$\langle \sigma_1 \rangle = \langle \sigma_2 \rangle, \qquad M_1 = M_2, \qquad Z_{\tilde{K}} = Z_{\tilde{K}^\pm} = Z_{\tilde{K}^0}, \qquad Z_{\tilde{\pi}} = Z_{\tilde{\pi}^\pm} = Z_{\tilde{\pi}^0}, \qquad (22)$$

where Zs are the wave function renormalization constants given in (B8), and σ_i in Sec. IV stand for $\tilde{\sigma}_i$. This is because, we have to assume at least $SU(2)_V$ for a realistic parameter space as we will see.

(i) ϕ-ϕ-γ

[4]Since $SU(3)_V$ is unbroken, all the DM particles have the mass which is denoted by $m_{\rm DM}$ here.

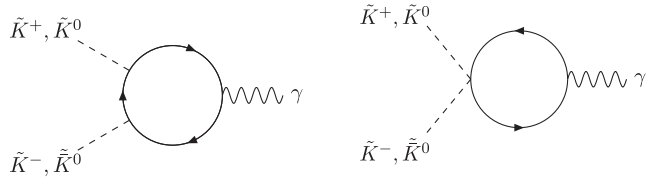

FIG. 3. The ϕ-ϕ-γ coupling (charge radius), which vanishes in the $SU(3)_V$ limit. The $\tilde{\pi}$-$\tilde{\pi}$-γ coupling vanishes in the $SU(2)_V$ limit.

The corresponding one-loop diagram is shown in Fig. 3, where the right diagram in Fig. 3 yields zero contribution.

$$\begin{aligned}\mathcal{L}_{\phi^2\gamma} = A^{\mu\nu}&(G_{K^+K^-\gamma}\partial_\mu\tilde{K}^+\partial_\nu\tilde{K}^- + G_{K^0\bar{K}^0\gamma}\partial_\mu\tilde{K}^0\partial_\nu\tilde{\bar{K}}^0 \\ &+ G_{\pi^+\pi^-\gamma}\partial_\mu\tilde{\pi}^+\partial_\nu\tilde{\pi}^-) \\ &+ Z^{\mu\nu}(G_{K^+K^-Z}\partial_\mu\tilde{K}^+\partial_\nu\tilde{K}^- + G_{K^0\bar{K}^0Z}\partial_\mu\tilde{K}^0\partial_\nu\tilde{\bar{K}}^0 \\ &+ G_{\pi^+\pi^-Z}\partial_\mu\tilde{\pi}^+\partial_\nu\tilde{\pi}^-),\end{aligned} \tag{23}$$

where $A(Z)_{\mu\nu} = \partial_\mu A(Z)_\nu - \partial_\nu A(Z)_\mu$. The effective couplings in the large Λ limit are

$$\begin{aligned}G_{K^+K^-\gamma} &= 2Z_{\tilde{K}^\pm}n_c eQ\left(1-\frac{G_D}{8G^2}\langle\sigma_2\rangle\right)^2 I_{\phi^2\gamma}(M_3,M_1), \\ G_{K^0\bar{K}^0\gamma} &= 2Z_{\tilde{K}^0}n_c eQ\left(1-\frac{G_D}{8G^2}\langle\sigma_1\rangle\right)^2 I_{\phi^2\gamma}(M_3,M_2), \\ G_{\pi^+\pi^-\gamma} &= 2Z_{\tilde{\pi}^\pm}n_c eQ\left(1-\frac{G_D}{8G^2}\langle\sigma_3\rangle\right)^2 I_{\phi^2\gamma}(M_2,M_1), \\ G_{K^+K^-Z} &= -t_W G_{K^+K^-\gamma}, \qquad G_{K^0\bar{K}^0Z} = -t_W G_{K^0\bar{K}^0\gamma}, \\ G_{\pi^+\pi^-Z} &= -t_W G_{\pi^+\pi^-\gamma},\end{aligned} \tag{24}$$

$t_W^2 = (\sin\theta_W/\cos\theta_W)^2 \simeq 0.3$, and $I_{\phi\gamma^2}(m_a,m_b)$ is given in (C4). In the $SU(2)_V$ limit, we obtain $G_{K^0\bar{K}^0\gamma} = G_{K^+K^-\gamma}$ and $G_{\pi^+\pi^-\gamma} = 0$, because $I_{\phi^2\gamma}(m_a,m_b) \to (m_b - m_a)/(48\pi^2 m_a^3)$ as $m_b \to m_a$.

(ii) $\phi \to \gamma\gamma$

The diagram in Fig. 4 shows the decay of $\tilde{\eta}$, $\tilde{\pi}^0$ and S into two γs, but they can also decay two Zs and γ and Z, if the processes are kinematically allowed. Using the NJL Lagrangian (A2) and (C5) in Appendix C we find that the effective interaction takes the form

$$\begin{aligned}\mathcal{L}_{\phi\gamma^2} = &\frac{1}{4}\tilde{\eta}\epsilon^{\mu\nu\alpha\beta}\left(\frac{1}{2}G_{\eta\gamma^2}A_{\mu\nu}A_{\alpha\beta} + G_{\eta\gamma Z}A_{\mu\nu}Z_{\alpha\beta} + \frac{1}{2}G_{\eta Z^2}Z_{\mu\nu}Z_{\alpha\beta}\right) \\ &+ \frac{1}{4}\tilde{\pi}^0\epsilon^{\mu\nu\alpha\beta}\left(\frac{1}{2}G_{\pi^0\gamma^2}A_{\mu\nu}A_{\alpha\beta} + G_{\pi^0\gamma Z}A_{\mu\nu}Z_{\alpha\beta} + \frac{1}{2}G_{\pi^0 Z^2}Z_{\mu\nu}Z_{\alpha\beta}\right),\end{aligned} \tag{25}$$

where in the large Λ limit

$$G_{\eta\gamma^2} = Z_{\tilde{\eta}}^{1/2}n_c\frac{\alpha}{\sqrt{3}\pi}Q^2\left[\left(1-\frac{G_D}{8G^2}(2\langle\sigma_2\rangle - \langle\sigma_3\rangle)\right)M_1^{-1} + \left(1-\frac{G_D}{8G^2}(2\langle\sigma_1\rangle - \langle\sigma_3\rangle)\right)M_2^{-1} - \left(2-\frac{G_D}{8G^2}(\langle\sigma_1\rangle + \langle\sigma_2\rangle)\right)M_3^{-1}\right], \tag{26}$$

$$\begin{aligned}&G_{\eta\gamma Z} = -t_W G_{\eta\gamma^2}, \qquad G_{\eta Z^2} = t_W^2 G_{\eta\gamma^2}, \\ &G_{\pi^0\gamma^2} = Z_{\tilde{\pi}}^{1/2}n_c\frac{\alpha}{\pi}Q^2\left(1-\frac{G_D}{8G^2}\langle\sigma_3\rangle\right)(M_1^{-1} - M_2^{-1}), \\ &G_{\pi^0\gamma Z} = -t_W G_{\pi^0\gamma^2}, \qquad G_{\pi^0 Z^2} = t_W^2 G_{\pi^0\gamma^2}.\end{aligned} \tag{27}$$

As we see from (27), the $\tilde{\pi}^0 \to \gamma\gamma$ decay vanishes in the $SU(2)_V$ limit, because $M_1 = M_2$ in this limit.

The decay of S into two γ, two Z, and γZ can be described by

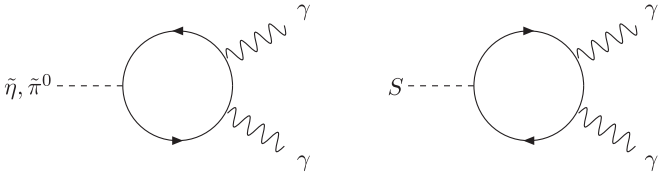

FIG. 4. Decay of DM and S into two γs. In the $SU(2)_V$ limit $\tilde{\pi}^0$ does not decay.

$$\mathcal{L}_{S\gamma^2} = S\left(\frac{1}{2}G_{S\gamma^2}A_{\mu\nu}A^{\mu\nu} + G_{S\gamma Z}A_{\mu\nu}Z^{\mu\nu} + \frac{1}{2}G_{SZ^2}Z_{\mu\nu}Z^{\mu\nu}\right), \tag{28}$$

where we find from (D8)

$$G_{S\gamma^2} = \frac{\alpha}{3\pi}Q^2\sum_{i=1,2,3}y_i M_i^{-1}, \tag{29}$$

$$G_{S\gamma Z} = -t_W G_{S\gamma^2}, \qquad G_{SZ^2} = t_W^2 G_{S\gamma^2}. \tag{30}$$

(iii) Dark matter conversion

The diagrams in Figs. 5 and 6 are examples of DM conversion, in which two incoming DM particles are annihilated into a pair of two DM particles which are different from the incoming ones. There are DM conversion amplitudes, which do not vanish in the $SU(3)_V$ limit, and those which vanish in the limit. Except the last $\eta K^2\pi$ interaction term, the effective interaction term below do not vanish the $SU(3)_V$ limit.

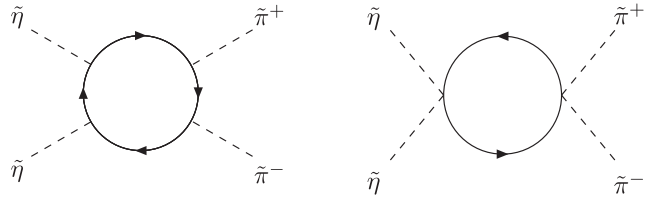

FIG. 5. Examples for DM conversion.

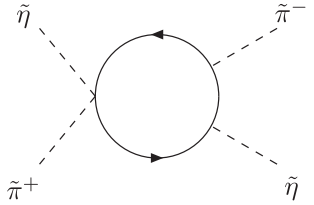

FIG. 6. This DM conversion vanishes in the $SU(3)_V$ limit.

$$\mathcal{L}_{\phi^4} = \frac{1}{2}G_{\eta^2K^2}\tilde{\eta}^2(\tilde{K}^0\tilde{\bar{K}}^0 + \tilde{K}^+\tilde{K}^-) + \frac{1}{2}G_{\eta^2\pi^2}\tilde{\eta}^2\left(\frac{1}{2}(\tilde{\pi}^0)^2 + \tilde{\pi}^+\tilde{\pi}^-\right) + G_{K^2\pi^2}(\tilde{K}^0\tilde{\bar{K}}^0 + \tilde{K}^+\tilde{K}^-)\left(\frac{1}{2}(\tilde{\pi}^0)^2 + \tilde{\pi}^+\tilde{\pi}^-\right) + G_{\eta K^2\pi}\tilde{\eta}((\tilde{K}^0\tilde{\bar{K}}^0 - \tilde{K}^+\tilde{K}^-)\tilde{\pi}^0 + \sqrt{2}\tilde{K}^0\tilde{K}^-\tilde{\pi}^+ + \sqrt{2}\tilde{\bar{K}}^0\tilde{K}^+\tilde{\pi}^-), \quad (31)$$

where

$$G_{\eta^2K^2} = \frac{4}{3}Z_{\tilde{\eta}}Z_{\tilde{K}}n_c\left(1-\frac{G_D}{8G^2}\langle\sigma_1\rangle\right)^2\left[\left(1-\frac{G_D}{8G^2}(2\langle\sigma_1\rangle-\langle\sigma_3\rangle)\right)^2 I^{2A}_{\phi^4}(M_1,M_3) + 4\left(1-\frac{G_D}{8G^2}\langle\sigma_1\rangle\right)^2 I^{2A}_{\phi^4}(M_3,M_1) - 2\left(1-\frac{G_D}{8G^2}\langle\sigma_1\rangle\right)\left(1-\frac{G_D}{8G^2}(2\langle\sigma_1\rangle-\langle\sigma_3\rangle)\right) I^{1A}_{\phi^4}(M_1,M_3)\right] + \frac{4}{3}Z_{\tilde{\eta}}Z_{\tilde{K}}n_c\left(\frac{G_D}{8G^2}\right)^2(I^{1B}_{\phi^4}(M_1,M_3) + 2I^{2B}_{\phi^4}(M_1)), \quad (32)$$

$$G_{\eta^2\pi^2} = 4Z_{\tilde{\eta}}Z_{\tilde{\pi}}n_c\left(1-\frac{G_D}{8G^2}\langle\sigma_3\rangle\right)^2\left(1-\frac{G_D}{8G^2}(2\langle\sigma_1\rangle-\langle\sigma_3\rangle)\right)^2 I^{3A}_{\phi^4}(M_1) + \frac{4}{3}Z_{\tilde{\eta}}Z_{\tilde{\pi}}n_c\left(\frac{G_D}{8G^2}\right)^2(4I^{2B}_{\phi^4}(M_1) - I^{2B}_{\phi^4}(M_3)), \quad (33)$$

$$G_{K^2\pi^2} = 4Z_{\tilde{K}}Z_{\tilde{\pi}}n_c\left(1-\frac{G_D}{8G^2}\langle\sigma_1\rangle\right)^2\left(1-\frac{G_D}{8G^2}\langle\sigma_3\rangle\right)^2 I^{2A}_{\phi^4}(M_1,M_3) + 4Z_{\tilde{\pi}}Z_{\tilde{K}}n_c\left(\frac{G_D}{8G^2}\right)^2 I^{1B}_{\phi^4}(M_1,M_3), \quad (34)$$

$$G_{\eta K^2\pi} = \frac{4}{\sqrt{3}}Z^{1/2}_{\tilde{\eta}}Z_{\tilde{K}}Z^{1/2}_{\tilde{\pi}}n_c\left(1-\frac{G_D}{8G^2}\langle\sigma_1\rangle\right)^2\left(1-\frac{G_D}{8G^2}\langle\sigma_3\rangle\right) \times\left[\left(1-\frac{G_D}{8G^2}\langle\sigma_1\rangle\right) I^{1A}_{\phi^4}(M_1,M_3) - \left(1-\frac{G_D}{8G^2}(2\langle\sigma_1\rangle-\langle\sigma_3\rangle)\right) I^{2A}_{\phi^4}(M_1,M_3)\right] + \frac{4}{\sqrt{3}}Z^{1/2}_{\tilde{\eta}}Z_{\tilde{K}}Z^{1/2}_{\tilde{\pi}}n_c\left(\frac{G_D}{8G^2}\right)^2(I^{1B}_{\phi^4}(M_1,M_3) - I^{2B}_{\phi^4}(M_1)), \quad (35)$$

and $I^{1A}_{\phi^4}(m_a,m_b)$, etc. are defined in (C8)–(C12) in Appendix C. We have not included the contributions from the diagram like one in Fig. 6, because they are negligibly suppressed in a realistic parameter space, in which $SU(3)_V$ is only weakly broken. Similarly, $G_{\eta K^2\pi}$, too, is negligibly small ($G_{\eta K^2\pi}/G_{\eta^2K^2} \sim 10^{-4}$), so that we will not take into account the $\eta K^2\pi$ interactions in computing the DM relic abundance.

(iv) Dark matter coupling with S

The diagrams in Figs. 7 and 8 show dark matter interactions with the singlet S. The DM coupling with S (Fig. 7) can be described by

$$\mathcal{L}_{\phi^2S} = S\left(\frac{1}{2}G_{\eta^2S}\tilde{\eta}^2 + +G_{K^2S}(\tilde{K}^0\tilde{\bar{K}}^0 + \tilde{K}^+\tilde{K}^-) + G_{\pi^2S}\left(\frac{1}{2}(\tilde{\pi}^0)^2 + \tilde{\pi}^+\tilde{\pi}^-\right)\right). \quad (36)$$

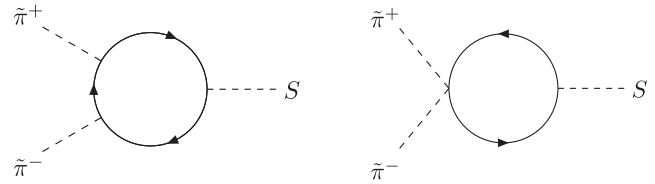

FIG. 7. DM coupling with one S. In a realistic parameter space there is an accidental cancellation between these two diagrams.

Using (C15)–(C17) in Appendix C we find in the large Λ limit

$$G_{\eta^2 S} = -\frac{2}{3} Z_{\tilde{\eta}} n_c \left[4y_1 \left(1 - \frac{G_D}{8G^2} (2\langle\sigma_1\rangle - \langle\sigma_3\rangle) \right)^2 I^{2A}_{\phi^2 S}(M_1) + 2y_3 \left(1 - \frac{G_D}{8G^2} \langle\sigma_1\rangle \right)^2 I^{2A}_{\phi^2 S}(M_3) \right] - \frac{2}{3} Z_{\tilde{\eta}} n_c \left(\frac{G_D}{8G^2} \right) (4y_1 I^{B}_{\phi^2 S}(M_1) - y_3 I^{B}_{\phi^2 S}(M_3)), \tag{37}$$

$$G_{K^2 S} = -2Z_{\tilde{K}} n_c \left(1 - \frac{G_D}{8G^2} \langle\sigma_1\rangle \right)^2 (y_1 I^{1A}_{\phi^2 S}(M_3, M_1) + y_3 I^{1A}_{\phi^2 S}(M_1, M_3)) - 2Z_{\tilde{K}} n_c \left(\frac{G_D}{8G^2} \right) y_1 I^{B}_{\phi^2 S}(M_1), \tag{38}$$

$$G_{\pi^2 S} = -4Z_{\tilde{\pi}} n_c \left(1 - \frac{G_D}{8G^2} \langle\sigma_3\rangle \right)^2 y_1 I^{2A}_{\phi^2 S}(M_1) - 2Z_{\tilde{\pi}} n_c \left(\frac{G_D}{8G^2} \right) y_3 I^{B}_{\phi^2 S}(M_3). \tag{39}$$

The DM coupling with two Ss (Fig. 8) can be described by

$$\mathcal{L}_{\phi^2 S^2} = \frac{1}{2} S^2 \left(\frac{1}{2} G_{\eta^2 S^2} \tilde{\eta}^2 + + G_{K^2 S^2} (\tilde{K}^0 \tilde{\bar{K}}^0 + \tilde{K}^+ \tilde{K}^-) + G_{\pi^2 S^2} \left(\frac{1}{2} (\tilde{\pi}^0)^2 + \tilde{\pi}^+ \tilde{\pi}^- \right) \right), \tag{40}$$

where

$$G_{\eta^2 S^2} = -\frac{2}{3} Z_{\tilde{\eta}} n_c \left[y_1^2 \left(1 - \frac{G_D}{8G^2} (2\langle\sigma_1\rangle - \langle\sigma_3\rangle) \right)^2 (2I^{2A}_{\phi^2 S^2}(M_1) + I^{2B}_{\phi^2 S^2}(M_1)) + 2y_3^2 \left(1 - \frac{G_D}{8G^2} \langle\sigma_1\rangle \right)^2 (2I^{2A}_{\phi^2 S^2}(M_3) + I^{2B}_{\phi^2 S^2}(M_3)) \right] - \frac{1}{3} Z_{\tilde{\eta}} n_c \left(\frac{G_D}{8G^2} \right) (4y_1^2 I^{C}_{\phi^2 S^2}(M_1) - y_3^2 I^{C}_{\phi^2 S^2}(M_3)), \tag{41}$$

$$G_{K^2 S^2} = -2Z_{\tilde{K}} n_c \left(1 - \frac{G_D}{8G^2} \langle\sigma_1\rangle \right)^2 (y_1^2 I^{1A}_{\phi^2 S^2}(M_3, M_1) + y_3^2 I^{1A}_{\phi^2 S^2}(M_1, M_3) + y_1 y_3 I^{1B}_{\phi^2 S^2}(M_1, M_3)) - Z_{\tilde{K}} n_c \left(\frac{G_D}{8G^2} \right) y_1^2 I^{C}_{\phi^2 S^2}(M_1), \tag{42}$$

$$G_{\pi^2 S^2} = -2Z_{\tilde{\pi}} n_c \left(1 - \frac{G_D}{8G^2} \langle\sigma_3\rangle \right)^2 y_1^2 (2I^{2A}_{\phi^2 S^2}(M_1) + I^{2B}_{\phi^2 S^2}(M_1)) - Z_{\tilde{\pi}} n_c \left(\frac{G_D}{8G^2} \right) y_3^2 I^{C}_{\phi^2 S^2}(M_3). \tag{43}$$

(v) Dark matter coupling with two γs

The diagram in Fig. 9 shows the annihilation of $\pi^\pm$ pair into two γs, where the annihilations into γZ, two Zs, and also into two Ss are also possible if they are kinematically allowed.

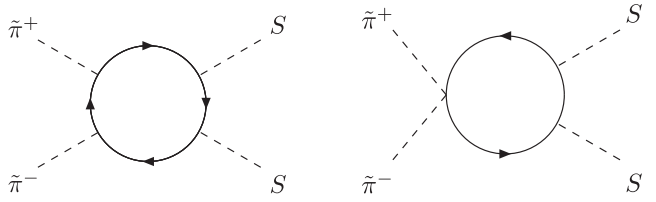

FIG. 8. DM coupling with two Ss. These diagrams contribute to the DM relic abundance if the mass of S is comparable with or less than the DM masses.

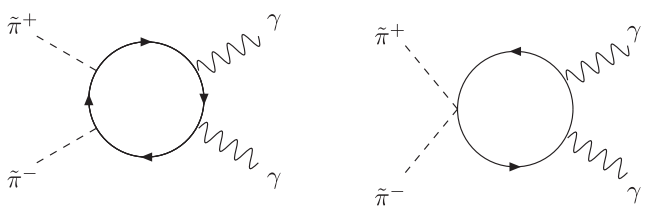

FIG. 9. DM annihilation into two γs.

$$\mathcal{L}_{\phi^2G^2} = \frac{1}{4}A_{\mu\nu}A^{\mu\nu}\left(G_{\eta^2\gamma^2}\frac{1}{2}(\tilde{\eta})^2 + G_{K^2\gamma^2}(\tilde{K}^0\tilde{\bar{K}}^0 + \tilde{K}^+\tilde{K}^-) + G_{\pi^2\gamma^2}\left(\frac{1}{2}(\tilde{\pi}^0)^2 + \tilde{\pi}^+\tilde{\pi}^-\right)\right)$$
$$+\frac{1}{2}A_{\mu\nu}Z^{\mu\nu}\left(G_{\eta^2\gamma Z}\frac{1}{2}(\tilde{\eta})^2 + G_{K^2\gamma Z}(\tilde{K}^0\tilde{\bar{K}}^0 + \tilde{K}^+\tilde{K}^-) + G_{\pi^2\gamma Z}\left(\frac{1}{2}(\tilde{\pi}^0)^2 + \tilde{\pi}^+\tilde{\pi}^-\right)\right)$$
$$+\frac{1}{4}Z_{\mu\nu}Z^{\mu\nu}\left(G_{\eta^2Z^2}\frac{1}{2}(\tilde{\eta})^2 + G_{K^2Z^2}(\tilde{K}^0\tilde{\bar{K}}^0 + \tilde{K}^+\tilde{K}^-) + G_{\pi^2Z^2}\left(\frac{1}{2}(\tilde{\pi}^0)^2 + \tilde{\pi}^+\tilde{\pi}^-\right)\right), \tag{44}$$

where $A(Z)_{\mu\nu} = \partial_\mu A(Z)_\nu - \partial_\nu A(Z)_\mu$. Using the approximate form (C29) and (C30) we find

$$G_{\eta^2\gamma^2} = Z_{\tilde{\eta}}n_c\frac{\alpha}{\pi}Q^2\mathcal{A}_{\tilde{\eta}}(\gamma\gamma) \simeq Z_{\tilde{\eta}}n_c\frac{\alpha}{\pi}Q^2\mathcal{A}_{\tilde{\pi}}(\gamma\gamma), \tag{45}$$

$$G_{\eta^2\gamma Z} = -t_W G_{\eta^2\gamma^2}, \qquad G_{\eta^2Z^2} = t_W^2 G_{\eta^2\gamma^2},$$
$$G_{K^2\gamma^2} = Z_{\tilde{K}}n_c\frac{\alpha}{\pi}Q^2\mathcal{A}_{\tilde{K}}(\gamma\gamma) \simeq Z_{\tilde{K}}n_c\frac{\alpha}{\pi}Q^2\mathcal{A}_{\tilde{\pi}}(\gamma\gamma),$$
$$G_{K^2\gamma Z} = -t_W G_{K^2\gamma^2}, \qquad G_{K^2Z^2} = t_W^2 G_{K^2\gamma^2},$$
$$G_{\pi^2\gamma^2} = Z_{\tilde{\pi}}n_c\frac{\alpha}{\pi}Q^2\mathcal{A}_{\tilde{\pi}}(\gamma\gamma),$$
$$G_{\pi^2\gamma Z} = -t_W G_{\pi^2\gamma^2}, \qquad G_{\pi^2Z^2} = t_W^2 G_{\pi^2\gamma^2}, \tag{46}$$

where

$$\mathcal{A}_{\tilde{\pi}}(\gamma\gamma) = \frac{4}{3}\left[-\left(1 - \frac{G_D}{8G^2}\langle\sigma_3\rangle\right)^2 M_1^{-2} + \frac{G_D}{8G^2}M_3^{-1}\right], \tag{47}$$

and $\mathcal{A}_{\tilde{\eta}}(\gamma\gamma) = \mathcal{A}_{\tilde{K}}(\gamma\gamma) = \mathcal{A}_{\tilde{\pi}}(\gamma\gamma)$ in the $SU(3)_V$ limit. In a realistic parameter space for the $SU(2)_V$ case, the ratio $\mathcal{A}_{\tilde{\pi}}(\gamma\gamma)/\mathcal{A}_{\tilde{\eta}}(\gamma\gamma)$, for instance, is at most 1.004.

In the following discussions we shall use the effective interaction terms derived above to compute the DM relic abundance as well as the cross sections for the direct and indirect detections of DM.

C. Relic abundance of dark matter

The $SU(3)_V$ case (9) has been discussed in [51,52], and so we below consider only the (i) and (ii) cases, which are defined in (7) and (8), respectively. In a one-component DM system, the velocity-averaged annihilation cross section $\langle v\sigma\rangle$ should be $\sim 10^{-9}$ GeV^{-2} to obtain a realistic DM relic abundance $\Omega h^2 \simeq 0.12$. A rough estimate of the velocity-averaged annihilation cross section for DM conversion (Fig. 5) shows $\langle v\sigma(\tilde{\eta}\,\tilde{\eta} \to \tilde{\pi}^+\tilde{\pi}^-)\rangle \simeq 10^{-5}(1 - m_{\tilde{\pi}}^2/m_{\tilde{\eta}}^2)^{1/2}$ GeV^{-2}, where it vanishes if $SU(3)_V$ is unbroken. The reason for the large annihilation cross section for DM conversion is that the coupling of the hidden fermions to the hidden mesons is of $O(1)$: There is no coupling constant for the coupling as one can see from the NJL Lagrangian (A2). That is, the annihilation cross section for DM conversion is about four orders of magnitude larger than that in an ordinary case, unless the masses of the incoming and outgoing DMs are almost degenerate.

1. (i) $U(1)_{\tilde{B}'} \times U(1)_{\tilde{B}}$

There exists a problem for the $U(1)_{\tilde{B}'} \times U(1)_{\tilde{B}}$ case (7), which we will discuss now. As we have found in the previous subsection, the lightest NG boson in the $U(1)_{\tilde{B}'} \times U(1)_{\tilde{B}}$ case is always the lightest between the neutral ones within the one-loop analysis in the NJL approximation and that without of loss of generality we can assume it is $\tilde{\pi}^0$. Its dominant decay mode is into two γs. The decay width can be calculated from the effective Lagrangian (25):

$$\Gamma(\tilde{\pi}^0 \to \gamma\gamma) = \frac{9Z_{\tilde{\pi}}Q^4\alpha^2}{64\pi^3}m_{\tilde{\pi}^0}^3\left(1 - \frac{G_D}{8G^2}\langle\sigma_3\rangle\right)^2 \times (1/M_1 - 1/M_2)^2$$
$$\simeq 10^{-6} \times Q^4 m_{\tilde{\pi}^0}^3(1/M_1 - 1/M_2)^2, \tag{48}$$

which should be compared with the expansion rate H of the Universe at $T = m_{\tilde{\pi}^0}$,

$$\frac{\Gamma(\tilde{\pi}^0 \to \gamma\gamma)}{H} \simeq 7 \times 10^8 Q^4 (m_{\tilde{\pi}^0}/M_1)^3(\Delta M/M_1)^2[\mathrm{TeV}/M_1] + O(\Delta M^3), \tag{49}$$

where $\Delta M = M_1 - M_2$. Therefore, unless the $U(1)_Y$ charge Q of the hidden fermions is very small or the constituent fermion masses M_1 and M_2 are accurately fine-tuned (or both), $\tilde{\pi}^0$ decays immediately into two γs. Since the stable DM particles can annihilate into two $\tilde{\pi}^0$s with a huge DM conversion rate, there will be almost no DM left in the end. Since we want to assume neither a tinny Q nor accurately fine-tuned constituent fermion masses, we will not consider below the DM phenomenology based on the $U(1)_{\tilde{B}'} \times U(1)_{\tilde{B}}$ flavor symmetry.

2. (ii) $SU(2)_V \times U(1)_{\tilde{B}}$

Now we come to the case (ii) in (8), which means $y_1 = y_2 < y_3$. In this case the unstable NG boson is $\tilde{\eta}$ which can decay into two γs (and also into two Ss if it is kinematically allowed). Because of $SU(2)_V$, $\tilde{\pi}^0$ is now

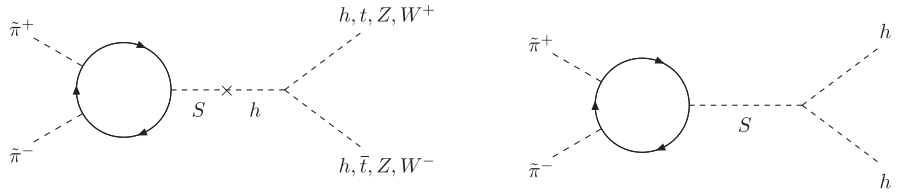

FIG. 10. DM annihilation into the SM particles via an internal S line and $S-h$ mixing. In the actual calculation of the cross section we use the localized expression for the one-loop part, i.e., $G_{\eta^2 S}$ etc. given in (37)–(39).

stable and $m_{\tilde{\pi}} = m_{\tilde{\pi}^0} = m_{\tilde{\pi}^\pm}$ [see (21)]. Furthermore, $m_{\tilde{K}^0}$ and $m_{\tilde{K}^\pm}$, which are slightly larger than $m_{\tilde{\pi}}$, are exactly degenerate in this case, i.e., $m_{\tilde{K}} = m_{\tilde{K}^\pm} = m_{\tilde{K}^0}$. In the parameter region (20) we can further constrain the parameter space. Since y is a measure of the explicit chiral symmetry breaking and at the same time is the strength of the connection to the SM side, the smaller is y, the smaller is the DM mass, and the larger is the cutoff Λ. We have also found that for a given set of λ_H, λ_{HS}, and λ_S the value $\langle S \rangle$ remains approximately constant as y varies, implying that m_S also remains approximately constant because the Higgs mass $m_h \simeq 126$ GeV and $v_h = \langle h \rangle \simeq 246$ GeV have to have a fixed value whatever y is. Consequently, the DM masses are smaller than m_S, unless $y_i \gtrsim 0.015$ or λ_S and λ_{HS} are very small (or both). We have found, as long as we assume (20), that $\lambda_S \lesssim 0.03$ and $\lambda_{HS} \lesssim 0.04$ have to be satisfied to realize that S is lighter than DM. However, these values of λ_S and λ_{HS} are too small for the DM annihilation cross sections into two Ss (diagrams in Fig. 8) to make the DM relic abundance realistic. In summary, there are three groups of DM in the $SU(2)_V$ case (8); the heaviest decaying $SU(2)_V$ singlet $\tilde{\eta}$, two $SU(2)_V$ doublet $(\{\tilde{\bar{K}}^0, \tilde{K}^-\}, \{\tilde{K}^+, \tilde{K}^0\})$ and lightest $SU(2)_V$ triplet $(\tilde{\pi}^\pm, \tilde{\pi}^0)$.

Before we compute the DM relic abundance, let us simplify the DM notion:

$$\chi_1 = \tilde{\eta}, \chi_2 \text{ to represent } \tilde{\bar{K}}^0, \tilde{K}^\pm, \tilde{K}^0, \chi_3 \text{ to represent } \tilde{\pi}^\pm, \tilde{\pi}^0 \tag{50}$$

with the masses

$$m_1 = m_{\tilde{\eta}}, \qquad m_2 = m_{\tilde{K}} \quad \text{and}$$
$$m_3 = m_{\tilde{\pi}} (m_1 > m_2 > m_3), \tag{51}$$

respectively, where χ_i are real scalar fields. There are three types of annihilation processes which enter into the Boltzmann equation:

$$\chi_i \chi_i \leftrightarrow XX, \tag{52}$$

$$\chi_i \chi_j \leftrightarrow \chi_k \chi_l, \tag{53}$$

in addition to the decay of χ_1 into two γs, where X stands for the SM particles, and the second process (53) is called DM conversion. There are two types of diagrams for the annihilation into the SM particles, Figs. 9 and 10. The diagrams in Fig. 10 are examples in which a one-loop diagram and a tree-diagram are connected by an internal S or a $S-h$ mixing. The same process can be realized by using the right diagram in Fig. 7 for the one-loop part. It turns out that there is an accidental cancellation between these two diagrams so that the velocity-averaged annihilation cross section is at most $\sim 10^{-11}$ GeV^{-2}, unless near the resonance in the s-channel [51]. The effective ϕ-ϕ-γ interaction (23) can also contribute to the s-channel annihilation into the SM particles. However, as we have mentioned, the effective coupling $G_{K^+K^-\gamma}$ is very small in the realistic parameter space. For instance, $m_{\tilde{K}}^3 G_{K^+K^-\gamma} / G_{K^2 S} \sim 10^{-5}$, where $G_{K^+K^-\gamma}$ and $G_{K^2 S}$ are given in (24) and (38), respectively. Note also that the DM conversion with three different DMs involved is forbidden by $SU(3)_V$. In the $SU(2)_V \times U(1)_{\tilde{B}}$ case, for instance, $\tilde{\eta}\tilde{\pi}^- \to \tilde{K}^0 \tilde{K}^-$ is indeed allowed. However, it is strongly suppressed $(G_{\eta K^2 \pi} / G_{\eta^2 K^2} \sim 10^{-4})$, because $SU(3)_V$ is only weakly broken in the realistic parameter space. So we will ignore this type of process, too, in the Boltzmann equation.

Using the notion for thermally averaged cross sections and decay width (of χ_1)

$$\langle v\sigma(ii; XX) \rangle, \qquad \langle v\sigma(ii; jj) \rangle, \qquad \langle \Gamma(1; \gamma\gamma) \rangle, \tag{54}$$

the reduced mass $1/\mu = (\sum_i m_i^{-1})$ and the inverse temperature $x = \mu/T$, we find for the number per comoving volume $Y_i = n_i/s$ [66]

$$\frac{dY_1}{dx} = -0.264 g_*^{1/2} \left[\frac{\mu M_{\rm PL}}{x^2}\right] \left\{ \langle v\sigma(11; XX) \rangle (Y_1 Y_1 - \bar{Y}_1 \bar{Y}_1) + \langle v\sigma(11; 22) \rangle \left(Y_1 Y_1 - \frac{Y_2 Y_2}{\bar{Y}_2 \bar{Y}_2} \bar{Y}_1 \bar{Y}_1 \right) + \langle v\sigma(11; 33) \rangle \left(Y_1 Y_1 - \frac{Y_3 Y_3}{\bar{Y}_3 \bar{Y}_3} \bar{Y}_1 \bar{Y}_1 \right) \right\} \tag{55}$$

$$- 0.602 g_*^{-1/2} \left[\frac{x M_{\rm PL}}{\mu^2}\right] \langle \Gamma(1;\gamma\gamma)\rangle (Y_1 - \bar{Y}_1),$$

$$\frac{dY_2}{dx} = -0.264 g_*^{1/2} \left[\frac{\mu M_{\rm PL}}{x^2}\right] \left\{ \langle v\sigma(22;XX)\rangle (Y_2 Y_2 - \bar{Y}_2 \bar{Y}_2) - \langle v\sigma(22;11)\rangle \left(Y_1 Y_1 - \frac{Y_2 Y_2}{\bar{Y}_2 \bar{Y}_2} \bar{Y}_1 \bar{Y}_1 \right) + \langle v\sigma(22;33)\rangle \left(Y_2 Y_2 - \frac{Y_3 Y_3}{\bar{Y}_3 \bar{Y}_3} \bar{Y}_2 \bar{Y}_2 \right) \right\}, \tag{56}$$

$$\frac{dY_3}{dx} = -0.264 g_*^{1/2} \left[\frac{\mu M_{\rm PL}}{x^2}\right] \left\{ \langle v\sigma(33;XX)\rangle (Y_3 Y_3 - \bar{Y}_3 \bar{Y}_3) - \langle v\sigma(33;11)\rangle \left(Y_1 Y_1 - \frac{Y_3 Y_3}{\bar{Y}_3 \bar{Y}_3} \bar{Y}_1 \bar{Y}_1 \right) - \langle v\sigma(33;22)\rangle \left(Y_2 Y_2 - \frac{Y_3 Y_3}{\bar{Y}_3 \bar{Y}_3} \bar{Y}_2 \bar{Y}_2 \right) \right\}, \tag{57}$$

where $g_* = 115.75$ is the total number of effective degrees of freedom, s is the entropy density, $M_{\rm PL}$ is the Planck mass, and $\bar{Y}_i = n_i/s$ in thermal equilibrium. Although $\langle v\sigma(ii;XX)\rangle$ is much smaller than 10^{-9} GeV^{-2}, we can obtain a realistic value of Ωh^2. The mechanism is the following [67]. If y_3 does not differ very much from $y_1 = y_2$, the differences among m_1, m_2, and m_3 are small. Then at finite temperature inverse DM conversions (which are kinematically forbidden at zero temperature) can become operative, because the DM conversions cross sections are large, i.e., 10^{-5} GeV$^{-2}\times$ phase space, as we have mentioned above. That is, the inverse conversion $\chi_3\chi_3, \chi_2\chi_2 \to \chi_1\chi_1 \to \gamma\gamma\gamma\gamma$ can play a significant role.

The relic abundance Ωh^2 is given by

$$\Omega_i h^2 = \frac{Y_{i\infty} s_0 m_i}{\rho_c/h^2}, \tag{58}$$

where $Y_{i\infty}$ is the asymptotic value of Y_i, $s_0 = 2890/\text{cm}^3$ is the entropy density at present, $\rho_c = 3H^2/8\pi G = 1.05\times 10^{-5} h^2$ GeV/cm^3 is the critical density, and h is the dimensionless Hubble parameter. Before we scan the parameter space, we consider a representative point in the four-dimensional parameter space with $Q = 1/3$:

$$y_3 = 0.00424, \qquad y_1 = y_2 = 0.00296,$$
$$\lambda_S = 0.13, \qquad \lambda_{HS} = 0.06, \qquad \lambda_H = 0.135, \tag{59}$$

which gives

$$\Omega h^2 = (\Omega_1 + 4\Omega_2 + 3\Omega_3)h^2 = 0.119, \qquad m_S = 324.1 \text{ GeV},$$
$$m_1 = m_{\tilde{\eta}} = 202.0 \text{ GeV}, \qquad m_2 = m_{\tilde{K}} = 196.3 \text{ GeV}, m_3 = m_{\tilde{\pi}} = 178.1 \text{ GeV},$$
$$\langle v\sigma(11,22,33;XX)\rangle = (9.29, 9.38, 1.26)\times 10^{-11} \text{ GeV}^{-2},$$
$$\langle v\sigma(11;22)\rangle = 4\langle v\sigma(22;11)\rangle = 3.90\times 10^{-5} \text{ GeV}^{-2},$$
$$\langle v\sigma(11;33)\rangle = 3\langle v\sigma(33;11)\rangle = 4.30\times 10^{-5} \text{ GeV}^{-2},$$
$$\langle v\sigma(22;33)\rangle = (3/4)\langle v\sigma(33;22)\rangle = 4.06\times 10^{-5} \text{ GeV}^{-2},$$
$$\langle \Gamma(1;\gamma\gamma)\rangle = 6.45\times 10^{-13} \text{ GeV}^{-1},$$
$$\langle v\sigma(11;\gamma\gamma)\rangle = 6.59\times 10^{-14} \text{ GeV}^{-2} = 7.73\times 10^{-31} \text{ cm}^3 \text{ s}^{-1}.$$

Fig. 11 (left) shows Ωh^2 (red (gray)), $\Omega_1 h^2 = \Omega_\eta h^2$ (black), $4\Omega_2 h^2 = 4\Omega_K h^2$ (green (gray line between the black and dashed gray lines)), and $3\Omega_3 h^2 = 3\Omega_\pi h^2$ (blue (gray)) for the parameter values (59) as a function of the inverse temperature $x = \mu/T$. In Fig. 11 (right) we show the total relic DM abundance Ωh^2 as a function of $y_1 (= y_2)$, where the other parameters are fixed as (59). Since a realistic value of Ωh^2 for the $SU(3)_V$ case (9) can be obtained only near the resonance, i.e., $m_S/m_{\rm DM} \simeq 2$, the parameter space for the $SU(2)_V$ case (8) is considerably larger than that for the $SU(3)_V$ case (9). Note, however, that the realistic parameter space for the $SU(2)_V$ case is not continuously connected to that for the $SU(3)_V$ case, as we can see from Fig. 11 (right) [$SU(3)_V$ means the point at $y_1 = y_3$].

D. Indirect and direct detection of dark matter

1. Monochromatic γ-ray line from DM annihilation

As we can see from Fig. 9, two DM particles can annihilate into two γs. Therefore, the charge Q of the hidden fermions can be constrained from the γ-ray observations [68–70]. Since in the $SU(2)_V$ case the relic abundance of the $\tilde{\pi}$ dark matter is dominant, we consider here only its annihilation into two γs. We will take into

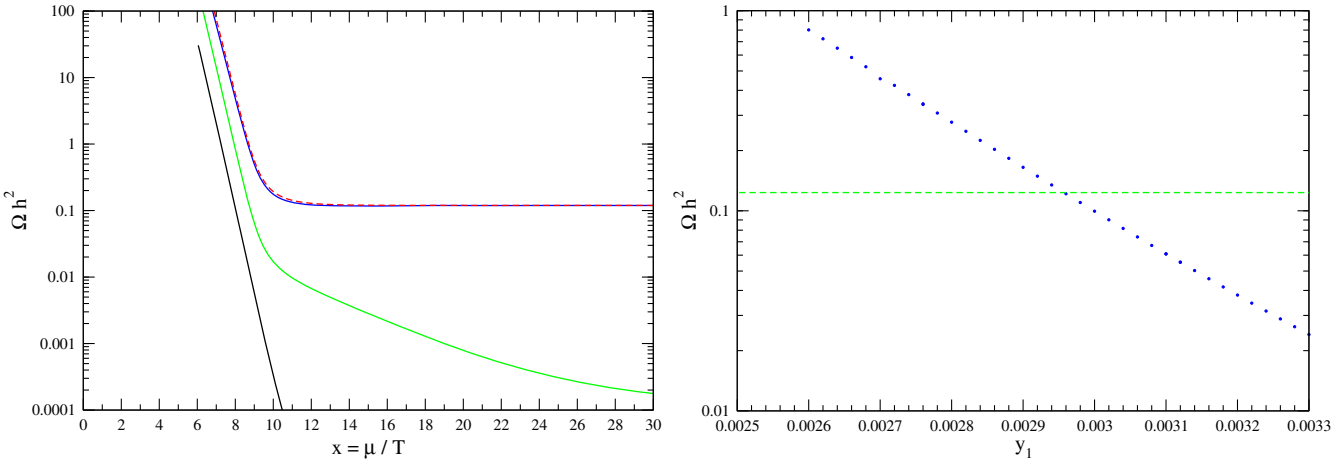

FIG. 11 (color online). Left: The relic DM abundances, Ωh^2 (red (dashed gray)), $\Omega_1 h^2 = \Omega_\eta h^2$ (black), $4\Omega_2 h^2 = 4\Omega_K h^2$ (green (gray line between the black and dashed gray lines)), and $3\Omega_3 h^2 = 3\Omega_\pi h^2$ (blue (gray)), as a function of the inverse temperature $x = \mu/T$ for the parameter values (59). Though $\tilde{\eta}$ is almost in thermal equilibrium, its presence is essential for the $\tilde{K}$ and $\tilde{\pi}$ numbers to decrease as x decreases. In the end the relic abundance of $\tilde{\pi}$ dominates. Right: The total relic abundance Ωh^2 as a function of $y_1 (= y_2)$ for $y_3 = 0.00424$, where the other parameters are fixed as (59).

account only the s-wave contribution to the annihilation cross section, and correspondingly we assume that $p = p' = (m_{\tilde{\pi}}, \mathbf{0})$ and that the photon momenta take the form $k = (m_{\tilde{\pi}}, \mathbf{k})$ and $k' = (m_{\tilde{\pi}}, -\mathbf{k})$ with their polarization tensors $\epsilon(k) = (0, \epsilon(k))$ and $\epsilon(k') = (0, \epsilon(k'))$ satisfying

$$0 = \epsilon(k)\cdot k = \epsilon(k)\cdot k' = \epsilon(k)\cdot p = \epsilon(k)\cdot p',$$
$$0 = \epsilon(k')\cdot k = \epsilon(k')\cdot k' = \epsilon(k')\cdot p = \epsilon(k')\cdot p', \quad (60)$$

respectively.

To compute the annihilation rate we use the effective interaction (44). We find that the annihilation amplitude can be written as

$$\Gamma_{\mu\nu}(ab) \simeq G_{\pi^2\gamma^2}(k\cdot k' g_{\mu\nu} - k_\mu k'_\nu) \times \begin{cases} & ab \\ 1 & \gamma\gamma \\ -t_W & \gamma Z \\ t_W^2 & ZZ \end{cases}, \quad (61)$$

where $G_{\pi^2\gamma^2}$ is given in (46). Then (the s-wave part of) the corresponding velocity-averaged annihilation cross sections are

$$\langle v\sigma(\tilde{\pi}\,\tilde{\pi} \to ab)\rangle = \frac{G_{\pi^2\gamma^2} m_{\tilde{\pi}}^2}{4\pi} \times \begin{cases} & ab \\ (1/2) & \gamma\gamma \\ t_W^2(1 - m_Z^2/4m_{\tilde{\pi}}^2) & \gamma Z \\ (3/4)t_W^4(1 - m_Z^2/m_{\tilde{\pi}}^2)^{1/2} & ZZ \end{cases}. \quad (62)$$

The energy E_γ of γ-ray line produced by the annihilation into γZ is $m_{\tilde{\pi}}(1 - m_Z^2/4m_{\tilde{\pi}}^2)$. In practice, however, due to finite detector energy resolution this line cannot be distinguished from the $E_\gamma = m_{\tilde{\pi}}$ line. Therefore, we simply add both cross sections. So we compute $\langle v\sigma\rangle_{\gamma\gamma+\gamma Z} = \langle v\sigma(\tilde{\pi}\,\tilde{\pi} \to \gamma\gamma)\rangle + \langle v\sigma(\tilde{\pi}\,\tilde{\pi} \to \gamma Z)\rangle$ with $Q = 1/3$ as a function of $m_{\tilde{\pi}}$ for different values of λ_H, λ_S, and λ_{HS}, which is shown in Fig. 12 (right), where Ωh^2 is required to be consistent with the PLANCK experiment at 4σ level [71]. As we see from Fig. 12 (right) the velocity-averaged annihilation cross section is mostly less than 10^{-29} cm^3/s in the parameter space we are considering, and consequently the Fermi LAT and HESS constraints given in Fig. 12 (left) are well satisfied. The red (gray) points are those for the $SU(3)_V$ (9) case.

The differential γ-ray flux is given by

$$\frac{d\Phi}{dE_\gamma} \propto \langle v\sigma\rangle_{\gamma\gamma}\frac{dN^{\gamma\gamma}}{dE_\gamma} + \langle v\sigma\rangle_{\gamma Z}\frac{dN^{\gamma z}}{dE_{\gamma Z}} \simeq \langle v\sigma\rangle_{\gamma\gamma+\gamma Z}\delta(E_\gamma - m_{\rm DM}). \quad (63)$$

Prospects observing such line spectrum is discussed in detail in [72–74]. Obviously, with an increasing energy resolution the chance for the observation increases. Observations of monochromatic γ-ray lines of energies of $O(100)$ GeV not only fix the charge of the hidden sector fermions, but also yields a first experimental hint on the hidden sector.

2. Direct detection of dark matter

As we can see from Fig. 11 (left), the relic abundance of the $\tilde{K}$ dark matter is about three orders of magnitude smaller than that of the $\tilde{\pi}$ dark matter. Therefore, we consider only the spin-independent elastic cross section

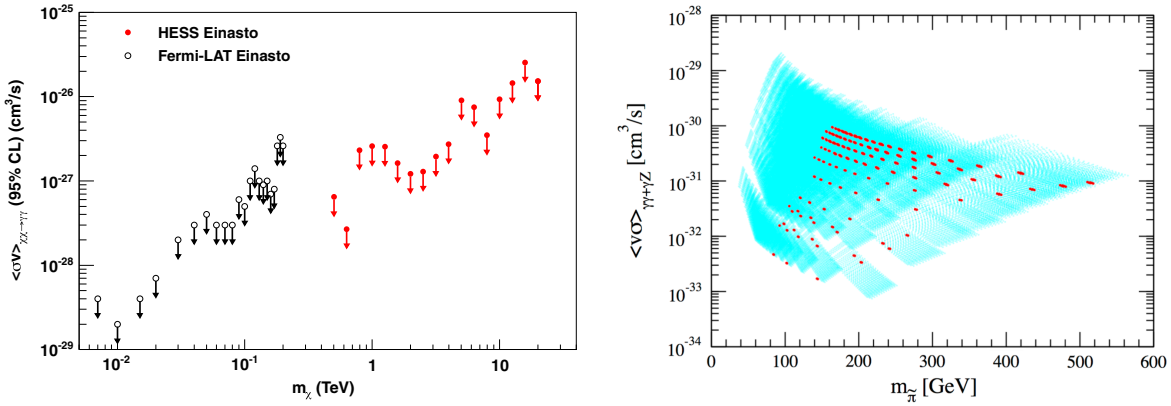

FIG. 12 (color online). Left: The Fermi Lat [68,69] (black) and HESS [70] (red (gray)) upper bounds on the velocity-averaged DM annihilation cross section for monochromatic γ-ray lines, where this graph is taken from [70]. Right: The velocity-averaged DM annihilation cross section $\langle v\sigma\rangle_{\gamma\gamma+\gamma Z}$ as a function of $m_{\tilde{\pi}}$ with $Q = 1/3$. Since $\langle v\sigma\rangle_{\gamma\gamma+\gamma Z}$ is proportional to Q^4, our calculations can be simply extended to the case of an arbitrary Q. The red (gray) points are those for the $SU(3)_V$ case (9).

$\sigma_{\rm SI}$ of $\tilde{\pi}$ off the nucleon. The subprocess is the left diagram in Fig. 13 (left), where • is the localized one-loop contribution (39), and we ignore the right diagram. The result of [75] can be used to find

$$\sigma_{\rm SI} = \frac{Z_{\tilde{\pi}}^2}{\pi} G_{\pi^2 S}^2 \left[\frac{\hat{f} m_N}{2 v_h m_{\tilde{\pi}}} \frac{\sin 2\theta}{2}\left(\frac{1}{m_h^2} - \frac{1}{m_S^2}\right)\right]^2 \left(\frac{m_N m_{\tilde{\pi}}}{m_N + m_{\tilde{\pi}}}\right)^2, \tag{64}$$

where $G_{\pi^2 S}$ is given in (39), m_N is the nucleon mass, and $\hat{f} \sim 0.3$ stems from the nucleonic matrix element [76]. We assume $|\cos\theta| \gtrsim 0.9$ to satisfy the LHC constraint, where θ is the $h - S$ mixing angle. In Fig. 13 (right) we show in the $m_{\tilde{\pi}}$-$\sigma_{\rm SI}$ plane the area in which $\Omega h^2 = 0.12 \pm 0.01(4\sigma)$ [71] is satisfied. The predicted values of $\sigma_{\rm SI}$ for $m_{\tilde{\pi}} \gtrsim 150$ GeV is too small even for the future direct DM detection experiment such as XENON1T, whose sensitivity is of $O(10^{-47})$ cm^2 [77]. The smallness of σ_{SI} results from the smallness of the coupling $G_{\pi^2 S}$, whose smallness comes from small Yukawa coupling y_1 and the accidental cancellation between the left and right diagrams in Fig. 7. The red (gray) points are those for the $SU(3)_V$ (9) case. We recall that the realistic parameter space for the $SU(2)_V$ case is not continuously connected to that for the $SU(3)_V$ case, as one could see from Fig. 11 (right), in which $y_1 = y_3$ has to be satisfied for the $SU(3)_V$ case.

If the relic abundance of the $\tilde{K}$ dark matter were of $O(0.1)$, the nonzero $\tilde{K}^0$-$\tilde{\bar{K}}^0$-γ/Z and $\tilde{K}^+$-$\tilde{K}^-$-γ/Z couplings shown in Fig. 13 would lead to a serious problem. Fortunately, the effective coupling is very small as we have already noticed: $m_{\tilde{K}}^2 G_{K^+K^-\gamma} \sim 10^{-6}$, where this coupling for $\tilde{\pi}$ vanishes in the $SU(2)_V$ case.

Note that because an accidental $U(1)_V$ (the hidden baryon number), not only the DM candidates, but also the lightest hidden baryons are stable. The hidden mesons in our model are neutral, while the charge of the hidden

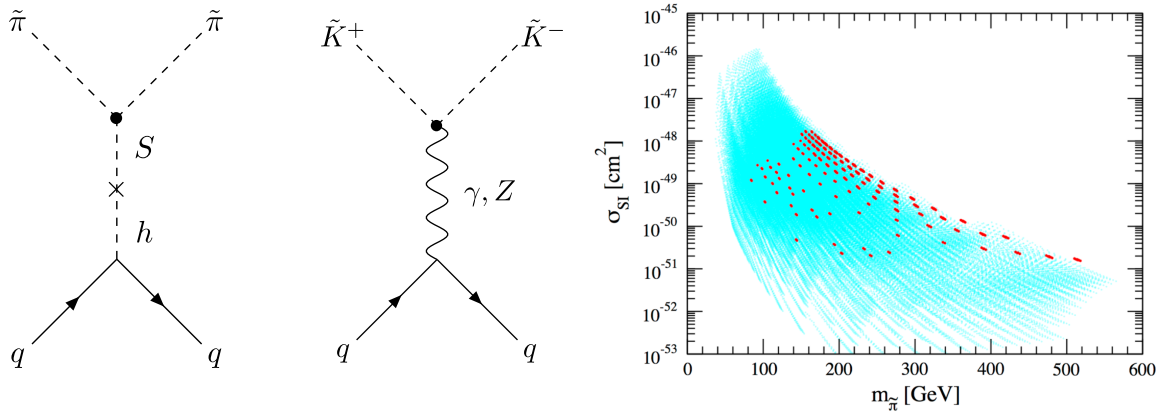

FIG. 13 (color online). Left: Subdiagrams contributing to the spin-independent elastic cross section $\sigma_{\rm SI}$ off the nucleon. Since the relic abundance of $\tilde{K}$ is negligibly small, the right diagram does not contribute. Right: The spin-independent elastic cross section $\sigma_{\rm SI}$ of $\tilde{\pi}$ as a function of $m_{\tilde{\pi}}$. The red (gray) points are those for the $SU(3)_V$ case (9). The result should be compared with the XENON1T sensitivity of $O(10^{-47})$ cm^2 [77].

baryons $\tilde{b}$ formed by three hidden fermions is $Q_{\tilde{b}} = 3 \times Q$. Let us roughly estimate the amount of relic stable hidden baryons and antibaryons in the Universe, where we assume that the hidden proton and neutron are the lightest baryons in the $SU(2)_V$ case (8). As the hidden sector is described by a scaled-up QCD, the hidden meson-baryon coupling $G_{\phi B\bar{B}}$ is approximately the same as in QCD, i.e., $G_{\phi B\bar{B}} \sim 13$, which is independent of Q. Using this fact, we can estimate $Y_{\tilde{b}} = n_{\tilde{b}}/s$ and obtain $Y_{\tilde{b}} \simeq (0.4, 6, 9) \times 10^{-16}$ for $m_{\tilde{b}} = 1, 5$ and 8 TeV, respectively. There are severe constraints on $Y_{\tilde{b}}$. The most severe constraints exist for $Q_{\tilde{b}} = 1$, which come from the search of heavy isotopes in sea water [4] and also from its influence on the large scale structure formation of the Universe [78]. We therefore conclude that $Q_{\tilde{b}} = 1$, i.e., $Q = 1/3$ is ruled out. Another severe cosmological constraint is due to catalyzed BBN [79], which gives $Y_{\tilde{b}} \lesssim 2 \times 10^{-15}$ [80] (see also [81]). The CMB constraint based on the Planck data is $\Omega_{\tilde{b}} h^2 \lesssim 0.001$ [82], which can be satisfied in our model if $m_{\tilde{b}} \lesssim 6$ TeV. (See also [83] in which the constraints in the $Q_{\tilde{b}}$-DM mass plane are given, where these constraints are satisfied in a wide area of the parameter space of the present model.).

In most of our analyses on DM here we have used $Q = 1/3$. The relic abundances of DMs depend on Q, because the decay rate of the neutral would-be DM η depends on Q. The change of Q can be compensated by varying the ratio of y_3 to $y_1 = y_2$, as far as the difference of two hypercharges are not very much different. As for the indirect detection of DM, the annihilation cross section into two γs (62) being proportional to Q^4 should be multiplied with $(3Q)^4$ for Q different from $1/3$. The spin-independent elastic cross section $\sigma_{\rm SI}$ (64) is independent on Q. This means that our basic results obtained in this paper can be simply extended to the case with Q different from $1/3$.

V. CONCLUSION

We have considered a QCD-like hidden sector model [48–51], in which dynamical chiral symmetry breaking generates a mass scale. This generated scale is transmitted to the SM sector via a real SM singlet scalar S to trigger spontaneous breaking of EW gauge symmetry [48,49]. Because the SM is extended in a classically scale invariant way, "Mass without mass" [1,84] is realized in this model. Since chiral symmetry is dynamically broken, there exist NG bosons, which are massive because the coupling of S with the hidden sector fermions breaks explicitly the $SU(n_f)_L \times SU(n_f)_R$ chiral symmetry down to one of its diagonal subgroups. The mass scale of these NG bosons is calculable once the strength of this coupling and the scale of the QCD-like hidden sector are given. The smallest subgroup is the Cartan subalgebra $U(1)^{n_f-1}$. Because of this (accidentally) unbroken subgroup, the NG bosons charged under $U(1)^{n_f-1}$ are stable: There exist at least $n_f^2 - n_f$ DM candidates. We have restricted ourselves to $n_c = n_f = 3$, because in this case we can relate using hadrons the independent parameters of the NJL model, which we have used as a low-energy effective theory for the hidden sector. There are three possibilities: (i) $U(1)_{\tilde{B}'} \times U(1)_{\tilde{B}}$, (ii) $SU(2)_V \times U(1)_{\tilde{B}}$, and (iii) $SU(3)_V$, where the possibility (iii) has been studied in [51,52]. It turns out that the first case (i) is unrealistic, unless this case is very close to (ii) or (iii), or/and the hypercharge Q of the hidden fermions is tiny. This is because the lightest NG boson is neutral under $U(1)_{\tilde{B}'} \times U(1)_{\tilde{B}}$ so that it can decay into two γs and the stable DM candidates annihilate into them immediately. Therefore, we have mainly studied the case (ii) with $y_1 = y_2 < y_3$. In this case the unstable NG boson is $\tilde{\eta}$ (the heaviest among the pseudo-NG bosons) and can decay into two γs. The annihilation cross section into the SM particles via the singlet S is very much suppressed, except in the resonance region in the s-channel annihilation diagram of DM. However, we have found another mechanism for the stable DMs to annihilate: If y_3 does not differ very much from $y_1 = y_2$, the differences among $m_{\tilde{\pi}}, m_{\tilde{K}}$, and $m_{\tilde{\eta}}$ are small. At finite temperature the inverse DM conversions (which are kinematically forbidden at zero temperature) can become operative, because the DM conversions cross sections are large $\sim 10^{-5}$ GeV^{-2}. Consequently, the realistic parameter space of the case (ii) is significantly larger than that of the case (iii), which has been obtained in [51,52].

With a nonzero Q the hidden sector is doubly connected with the SM sector; we have a bright hidden sector at hand. The connection via photon and Z opens possibilities to probe the hidden sector at collider experiments such as e^+e^- collision [85]. In particular, the would-be DM, $\tilde{\eta}$, can decay into two γs, which would give a smoking-gun event.

ACKNOWLEDGMENTS

We thank S. Matsumoto and H. Takano for useful discussions. The work of M. A. is supported in part by the Japan Society for the Promotion of Sciences (JSPS) Grant-in-Aid for Scientific Research (Grants No. 25400250 and No. 26105509).

APPENDIX A: THE NJL LAGRANGIAN IN THE SELF-CONSISTENT MEAN FIELD (SCMF) APPROXIMATION

Here we consider the NJL Lagrangian $\mathcal{L}_{\rm NJL}$ (13) in the SCMF approximation [58]. In the SCMF approximation one splits up the NJL Lagrangian (13) into the sum

$$\mathcal{L}_{\rm NJL} = \mathcal{L}_0 + \mathcal{L}_I, \tag{A1}$$

where $\mathcal{L}_I$ is normal ordered (i.e., $\langle 0|\mathcal{L}_I|0\rangle = 0$), and $\mathcal{L}_0$ contains at most fermion bilinears which are not normal ordered. We find that $\mathcal{L}_0$ can be written as

$$\mathcal{L}_0 = \mathcal{L}_K + \mathcal{L}_D + \mathcal{L}_M, \tag{A2}$$

where

$$\begin{aligned}
\mathcal{L}_K = {} & \mathrm{Tr}\bar{\psi}(i\gamma^\mu\partial_\mu + g'Q\gamma^\mu B_\mu)\psi - \left(\tilde{\sigma}_1 + y_1 S - \frac{G_D}{8G^2}\tilde{\sigma}_2\tilde{\sigma}_3\right)\bar{\psi}_1\psi_1 \\
& - \left(\tilde{\sigma}_2 + y_2 S - \frac{G_D}{8G^2}\tilde{\sigma}_1\tilde{\sigma}_3\right)\bar{\psi}_2\psi_2 - \left(\tilde{\sigma}_3 + y_3 S - \frac{G_D}{8G^2}\tilde{\sigma}_1\tilde{\sigma}_2\right)\bar{\psi}_3\psi_3 \\
& - i\left[\tilde{\pi}^0 + \frac{1}{\sqrt{3}}\tilde{\eta}^8 + \sqrt{\frac{2}{3}}\tilde{\eta}^0 - \frac{G_D}{8G^2}\left(\tilde{\sigma}_3\tilde{\pi}^0 + \frac{1}{\sqrt{3}}(2\tilde{\sigma}_2 - \tilde{\sigma}_3)\tilde{\eta}^8 - \sqrt{\frac{2}{3}}(\tilde{\sigma}_2 + \tilde{\sigma}_3)\tilde{\eta}^0\right)\right]\bar{\psi}_1\gamma_5\psi_1 \\
& - i\left[-\tilde{\pi}^0 + \frac{1}{\sqrt{3}}\tilde{\eta}^8 + \sqrt{\frac{2}{3}}\tilde{\eta}^0 - \frac{G_D}{8G^2}\left(-\tilde{\sigma}_3\tilde{\pi}^0 + \frac{1}{\sqrt{3}}(2\tilde{\sigma}_1 - \tilde{\sigma}_3)\tilde{\eta}^8 - \sqrt{\frac{2}{3}}(\tilde{\sigma}_1 + \tilde{\sigma}_3)\tilde{\eta}^0\right)\right]\bar{\psi}_2\gamma_5\psi_2 \\
& - i\sqrt{2}\tilde{\pi}^+\left(1 - \frac{G_D}{8G^2}\tilde{\sigma}_3\right)\bar{\psi}_1\gamma_5\psi_2 - i\sqrt{2}\tilde{\pi}^-\left(1 - \frac{G_D}{8G^2}\tilde{\sigma}_3\right)\bar{\psi}_2\gamma_5\psi_1 \\
& - i\sqrt{2}\tilde{K}^+\left(1 - \frac{G_D}{8G^2}\tilde{\sigma}_2\right)\bar{\psi}_1\gamma_5\psi_3 - i\sqrt{2}\tilde{K}^-\left(1 - \frac{G_D}{8G^2}\tilde{\sigma}_2\right)\bar{\psi}_3\gamma_5\psi_1 \\
& - i\sqrt{2}\tilde{K}^0\left(1 - \frac{G_D}{8G^2}\tilde{\sigma}_1\right)\bar{\psi}_2\gamma_5\psi_3 - i\sqrt{2}\bar{\tilde{K}}^0\left(1 - \frac{G_D}{8G^2}\tilde{\sigma}_1\right)\bar{\psi}_3\gamma_5\psi_2 \\
& - i\left[-\frac{2}{\sqrt{3}}\tilde{\eta}^8 + \sqrt{\frac{2}{3}}\tilde{\eta}^0 - \frac{G_D}{8G^2}\left((\tilde{\sigma}_1 - \tilde{\sigma}_2)\tilde{\pi}^0 - \frac{1}{\sqrt{3}}(\tilde{\sigma}_1 + \tilde{\sigma}_2)\tilde{\eta}^8 - \sqrt{\frac{2}{3}}(\tilde{\sigma}_1 + \tilde{\sigma}_2)\tilde{\eta}^0\right)\right]\bar{\psi}_3\gamma_5\psi_3,
\end{aligned} \tag{A3}$$

$$\begin{aligned}
\mathcal{L}_D = {} & \frac{G_D}{8G^2}\left[\left(2\tilde{K}^0\bar{\tilde{K}}^0 - \frac{2}{\sqrt{3}}\tilde{\pi}^0\tilde{\eta}^8 + \frac{2}{3}(\tilde{\eta}^8)^2 - \frac{2}{3}(\tilde{\eta}^0)^2\right)\bar{\psi}_1\psi_1 - \left(2\sqrt{\frac{2}{3}}\tilde{\pi}^+\tilde{\eta}^8 + 2\tilde{K}^+\bar{\tilde{K}}^0\right)\bar{\psi}_1\psi_2\right. \\
& - \left(2\sqrt{\frac{2}{3}}\tilde{\pi}^-\tilde{\eta}^8 + 2\tilde{K}^-\tilde{K}^0\right)\bar{\psi}_2\psi_1 + \left(2\tilde{K}^+\tilde{K}^- + \frac{2}{\sqrt{3}}\tilde{\pi}^0\tilde{\eta}^8 + \frac{2}{3}(\tilde{\eta}^8)^2 - \frac{2}{3}(\tilde{\eta}^0)^2\right)\bar{\psi}_2\psi_2 \\
& - \left(2\tilde{\pi}^+\tilde{K}^0 + \sqrt{2}\tilde{K}^+\left(\tilde{\pi}^0 - \frac{1}{\sqrt{3}}\tilde{\eta}^8\right)\right)\bar{\psi}_1\psi_3 - \left(2\tilde{\pi}^-\bar{\tilde{K}}^0 + \sqrt{2}\tilde{K}^-\left(\tilde{\pi}^0 - \frac{1}{\sqrt{3}}\tilde{\eta}^8\right)\right)\bar{\psi}_3\psi_1 \\
& - \left(2\tilde{\pi}^-\tilde{K}^+ - \sqrt{2}\tilde{K}^0\left(\tilde{\pi}^0 + \frac{1}{\sqrt{3}}\tilde{\eta}^8\right)\right)\bar{\psi}_2\psi_3 - \left(2\tilde{\pi}^+\tilde{K}^- - \sqrt{2}\bar{\tilde{K}}^0\left(\tilde{\pi}^0 + \frac{1}{\sqrt{3}}\tilde{\eta}^8\right)\right)\bar{\psi}_3\psi_2 \\
& + \left(2\tilde{\pi}^+\tilde{\pi}^- + (\tilde{\pi}^0)^2 - \frac{1}{3}(\tilde{\eta}^8)^2 - \frac{2}{3}(\tilde{\eta}^0)^2\right)\bar{\psi}_3\psi_3 \\
& + \sqrt{\frac{2}{3}}\tilde{\eta}^0\left\{\left(\tilde{\pi}^0 + \frac{1}{\sqrt{3}}\tilde{\eta}^8\right)\bar{\psi}_1\psi_1 + \sqrt{2}\tilde{\pi}^+\bar{\psi}_1\psi_2 + \sqrt{2}\tilde{K}^+\bar{\psi}_1\psi_3 + \sqrt{2}\tilde{\pi}^-\bar{\psi}_2\psi_1\right. \\
& \left.\left. + \left(-\tilde{\pi}^0 + \frac{1}{\sqrt{3}}\tilde{\eta}^8\right)\bar{\psi}_2\psi_2 + \sqrt{2}\tilde{K}^0\bar{\psi}_2\psi_3 + \sqrt{2}\tilde{K}^-\bar{\psi}_3\psi_1 + \sqrt{2}\bar{\tilde{K}}^0\bar{\psi}_3\psi_2 - \frac{2}{\sqrt{3}}\tilde{\eta}^8\bar{\psi}_3\psi_3\right\}\right],
\end{aligned} \tag{A4}$$

$$\begin{aligned}
\mathcal{L}_M = {} & -\frac{1}{8G}\left(\sum_{i=1}^{3}\tilde{\sigma}_i^2 + 2(\tilde{\eta}^0)^2 + 4\tilde{\pi}^+\tilde{\pi}^- + 4\tilde{K}^+\tilde{K}^- + 4\tilde{K}^0\bar{\tilde{K}}^0 + 2(\tilde{\pi}^0)^2 + 2(\tilde{\eta}^8)^2\right) \\
& + \frac{G_D}{16G^3}\left[\tilde{\sigma}_1\tilde{\sigma}_2\tilde{\sigma}_3 + \tilde{\sigma}_1\left(2\tilde{K}^0\bar{\tilde{K}}^0 + \frac{2}{3}(\tilde{\eta}^8)^2 - \frac{2}{3}(\tilde{\eta}^0)^2 - \frac{2}{\sqrt{3}}\tilde{\pi}^0\tilde{\eta}^8 + \sqrt{\frac{2}{3}}\tilde{\eta}^0\tilde{\pi}^0 + \frac{\sqrt{2}}{3}\tilde{\eta}^0\tilde{\eta}^8\right)\right. \\
& + \tilde{\sigma}_2\left(2\tilde{K}^+\tilde{K}^- + \frac{2}{3}(\tilde{\eta}^8)^2 - \frac{2}{3}(\tilde{\eta}^0)^2 + \frac{2}{\sqrt{3}}\tilde{\pi}^0\tilde{\eta}^8 - \sqrt{\frac{2}{3}}\tilde{\eta}^0\tilde{\pi}^0 + \frac{\sqrt{2}}{3}\tilde{\eta}^0\tilde{\eta}^8\right) \\
& \left. + \tilde{\sigma}_3\left(2\tilde{\pi}^+\tilde{\pi}^- + (\tilde{\pi}^0)^2 - \frac{1}{3}(\tilde{\eta}^8)^2 - \frac{2}{3}(\tilde{\eta}^0)^2 - \frac{2\sqrt{2}}{3}\tilde{\eta}^0\tilde{\eta}^8\right)\right].
\end{aligned} \tag{A5}$$

Here $\tilde{\eta}^0$ stands for ϕ_0, and the meson fields are defined in (4).

APPENDIX B: DETERMINATION OF THE NJL PARAMETERS G,G_D, AND Λ

As in [51] we apply the NJL Lagrangian (A2) with $g' = 0$ to describe the real hadrons, where we assume $SU(2)_V$ and replace $y_i S$ by the current quark masses, i.e., $y_1 S = y_2 S \to m_u$, $y_3 S \to m_s$. Then we compute the real meson masses $m_\pi, m_K, m_\eta, m_{\eta'}$ and decay constants f_π, f_K.

We obtain the following inverse meson propagators:

$$\Gamma_{\pi^\pm}(p^2) = \Gamma_{\pi^0}(p^2) = -\frac{1}{2G} + \frac{G_D}{8G^3}\sigma_3 + \left(1 - \frac{G_D}{8G^2}\sigma_3\right)^2 2n_c I^A_{\phi^2}(p^2, m_1, m_1) + \frac{G_D}{G^2} n_c I^B_{\phi^2}(m_3), \tag{B1}$$

$$\Gamma_{K^\pm}(p^2) = \Gamma_{\bar{K}^0 K^0}(p^2) = -\frac{1}{2G} + \frac{G_D}{8G^3}\sigma_1 + \left(1 - \frac{G_D}{8G^2}\sigma_1\right)^2 2n_c I^A_{\phi^2}(p^2, m_1, m_3) + \frac{G_D}{G^2} n_c I^B_{\phi^2}(m_1), \tag{B2}$$

$$\Gamma^8_\eta(p^2) = -\frac{1}{2G} + \frac{G_D}{6G^3}\left(\sigma_1 - \frac{1}{4}\sigma_3\right) + \frac{2}{3}\left(1 - \frac{G_D}{8G^2}(2\sigma_1 - \sigma_3)\right)^2 n_c I^A_{\phi^2}(p^2, m_1, m_1) + \frac{4}{3}\left(1 - \frac{G_D}{8G^2}\sigma_1\right)^2 n_c I^A_{\phi^2}(p^2, m_3, m_3) + \frac{4G_D}{3G^2} n_c I^B_{\phi^2}(m_1) - \frac{G_D}{3G^2} n_c I^B_{\phi^2}(m_3), \tag{B3}$$

$$\Gamma^0_\eta(p^2) = -\frac{1}{2G} - \frac{G_D}{12G^3}(2\sigma_1 + \sigma_3) + \left(1 + \frac{G_D}{8G^2}(\sigma_1 + \sigma_3)\right)^2 \frac{4}{3} n_c I^A_{\phi^2}(p^2, m_1, m_1) + \left(1 + \frac{G_D}{4G^2}\sigma_1\right)^2 \frac{2}{3} n_c I^A_{\phi^2}(p^2, m_3, m_3) - \frac{2G_D}{3G^2} n_c (2I^B_{\phi^2}(m_1) + I^B_{\phi^2}(m_3)), \tag{B4}$$

$$\Gamma_{\eta^8\eta^0}(p^2) = \frac{\sqrt{2}G_D}{24G^3}(\sigma_1 - \sigma_3) + \frac{2\sqrt{2}}{3}\left(1 - \frac{G_D}{8G^2}(2\sigma_1 - \sigma_3)\right)\left(1 + \frac{G_D}{8G^2}(\sigma_1 + \sigma_3)\right) n_c I^A_{\phi^2}(p^2, m_1, m_1) - \frac{2\sqrt{2}}{3}\left(1 - \frac{G_D}{8G^2}\sigma_1\right)\left(1 + \frac{G_D}{8G^2}(2\sigma_1)\right) n_c I^A_{\phi^2}(p^2, m_3, m_3) + \frac{\sqrt{2}G_D}{3G^2} n_c (I^B_{\phi^2}(m_1) - I^B_{\phi^2}(m_3)), \tag{B5}$$

where the integrals $I^A_{\phi^2}(p^2, m_a, m_b)$ and $I^B_{\phi^2}(m)$ are defined in Appendix (C2), and

$$m_1 = m_u + \sigma_1 - \frac{G_D}{8G^2}\sigma_1\sigma_3, \qquad m_3 = m_s + \sigma_3 - \frac{G_D}{8G^2}{\sigma_1}^2. \tag{B6}$$

The pion and kaon masses are the zeros of the inverse propagators, i.e.,

$$\Gamma_{\pi^\pm}(p^2 = {m_\pi}^2) = 0, \qquad \Gamma_{K^\pm}(p^2 = {m_K}^2) = 0, \tag{B7}$$

while the η and η' meson masses are obtained from the zero eigenvalues of the real part of the $\eta^8 - \eta^0$ mixing matrix. The wave function renormalization constants can be obtained from

$$Z_\pi{}^{-1} = \left.\frac{d\Gamma_{\pi^\pm}(p^2)}{dp^2}\right|_{p^2={m_\pi}^2}, \qquad Z_K{}^{-1} = \left.\frac{d\Gamma_{K^\pm}(p^2)}{dp^2}\right|_{p^2={m_K}^2}, \tag{B8}$$

and the pion and kaon decay constants are defined as

$$\langle 0|\mathrm{Tr}\bar{\psi}\gamma_\mu\gamma_5\frac{1}{2}(\sigma_1 + i\sigma_2)\psi|\pi^+(p)\rangle = i\sqrt{2}f_\pi p_\mu, \tag{B9}$$

$$\langle 0|\mathrm{Tr}\bar{\psi}\gamma_\mu\gamma_5\frac{1}{2}(\sigma_4 + i\sigma_5)\psi|K^+(p)\rangle = i\sqrt{2}f_K p_\mu. \tag{B10}$$

TABLE II. Values of the QCD NJL parameters obtained by fitting the pion and kaon decay constants and the meson masses, where we have assumed the $SU(2)_V$ flavor symmetry.

Parameter	$(2G^{\rm QCD})^{-1/2}$	$(-G_D^{\rm QCD})^{-1/5}$	$\Lambda^{\rm QCD}$	m_u	m_s
Value (MeV)	361	406	930	5.95	163

We use $m_\pi, m_K, m_\eta, m_{\eta'}, f_\pi$, and f_K to determine the QCD NJL parameters. The best fit values of the parameters are given in Table II. In Table III we compare the meson masses and decay constants calculated in the NJL theory with the experimental values. As we see from Table III, the NJL η mass is about 16% smaller than the experimental value. This seems to be a general feature of the NJL theory [58] (see also [86]).

TABLE III. Comparison of the NJL values with the corresponding experimental values.

	Theory (MeV)	Experimental value (MeV)
m_π	136	$140(\pi^\pm)135(\pi^0)$
m_K	499	$494(K^\pm)498(K^0,\bar{K}^0)$
m_η	460	548
$m_{\eta'}$	960	958
f_π	93	$92(\pi^-)$
f_K	105	$110(K^-)$

APPENDIX C: ONE-LOOP INTEGRALS

(i) Vacuum energy

To compute the effective potential (18) we need the vacuum energy

$$I_V(m)=\int\frac{d^4k}{i(2\pi)^4}\ln\det(\not k-m)$$
$$=\frac{1}{16\pi^2}\left(\Lambda^4\ln\left(1+\frac{m^2}{\Lambda^2}\right)-m^4\ln\left(1+\frac{\Lambda^2}{m^2}\right)+m^2\Lambda^2\right). \tag{C1}$$

(ii) Inverse propagator of dark matter

There are two types of diagrams which contribute to the inverse propagator of dark matter:

$$I^A_{\phi^2}(p^2,m_a,m_b)=\int\frac{d^4l}{i(2\pi)^4}\frac{\mathrm{Tr}(\not l-\not p+m_a)\gamma_5(\not l+m_b)\gamma_5}{((l-p)^2-m_a^2)(l^2-m_b^2)},$$
$$I^B_{\phi^2}(m)=\int\frac{d^4k}{i(2\pi)^4}\frac{m}{(k^2-m^2)}$$
$$=-\frac{1}{16\pi^2}m\left[\Lambda^2-m^2\ln\left(1+\frac{\Lambda^2}{m^2}\right)\right]. \tag{C2}$$

These expressions are used to find DM masses and wave function renormalization constants given in (B8), respectively.

(iii) ϕ-ϕ-γ amplitude

$$I^\mu_{\phi^2\gamma}(p,p',m_a,m_b)=(-1)\int\frac{d^4l}{i(2\pi)^4}\frac{\mathrm{Tr}(\not l+m_a)\gamma_5(\not l-\not p'+m_b)\gamma^\mu(\not l+\not p+m_b)\gamma_5}{((l+p)^2-m_b^2)(l^2-m_a^2)((l-p')^2-m_b^2)}+(p\leftrightarrow p',m_a\leftrightarrow m_b),$$
$$=-(p^\mu p'^\nu-p'^\mu p^\nu)(p+p')_\nu I_{\phi\gamma^2}(m_a,m_b)+\cdots \tag{C3}$$

with $p^2=p'^2$, where $\cdots$ stands for higher order terms in the expansion of the external momenta, and

$$I_{\phi^2\gamma}(m_a,m_b)=\frac{1}{8\pi^2}\frac{1}{(m_a^2-m_b^2)^2(m_a+m_b)^2}\left(\frac{1}{2}(m_a-m_b)(m_a^3+5m_a^2m_b+5m_am_b^2+m_b^3)\right.$$
$$\left.-\frac{1}{3}(m_a^4+3m_a^3m_b+m_a^2m_b^2+3m_am_b^3+m_b^4)\ln(m_a^2/m_b^2)^2\right). \tag{C4}$$

The effective ϕ-ϕ-γ interaction Lagrangian is given in (23).

(iv) ϕ-γ-γ amplitude

The $\phi(p)$-$\gamma(k)$-$\gamma(k')$ three-point function is needed to compute the decay $\tilde{\eta}$ into two γs (Fig. 4):

$$I^{\mu\nu}_{\phi\gamma^2}(k,k',m)=(-1)\int\frac{d^4l}{i(2\pi)^4}\frac{\mathrm{Tr}(\not l-\not k'+m)\gamma^\mu(\not l+m)\gamma^\nu(\not l+\not k+m)\gamma_5}{((l+k)^2-m^2)(l^2-m^2)((l-k')^2-m^2)}+(k\leftrightarrow k',\mu\leftrightarrow\nu)$$
$$=\frac{i}{4\pi^2m}\epsilon^{\mu\nu\alpha\beta}k_\alpha k'_\beta+\cdots \tag{C5}$$

The amplitude is thanks to γ_5 gauge invariant even for a finite Λ, i.e., $k_\nu I^{\mu\nu}_{\phi\gamma^2}(k,k',m) = k'_\mu I^{\mu\nu}_{\phi\gamma^2}(k,k',m) = 0$. The amplitude without γ_5 correspond to the $S(p)$-$\gamma(k)$-$\gamma(k')$ three-point function, which we denote by $I^{\mu\nu}_{0,S}(k,k',m)$. This amplitude is not gauge invariant so that we need to apply the least subtraction method [52]. The subscript 0 indicates that the amplitude is unsubtracted, and we denote the subtracted gauge-invariant one by $I^{\mu\nu}_S(k,k',m)$. In Appendix C we demonstrate how to use the least subtraction method for this case.

(v) ϕ-ϕ-ϕ-ϕ amplitude

The $\phi(p)$-$\phi(p')$-$\phi'(k)$-$\phi'(k')$- four-point function is needed to compute the DM conversion cross section (diagrams of Fig. 5):

$$I^A_{\phi^4}(p,p',k,k',m_a,m_b,m_c,m_d) = (-1)\int \frac{d^4l}{i(2\pi)^4}\frac{\mathrm{Tr}(\not{l}+m_a)\gamma_5(\not{l}-\not{p}'+m_b)\gamma_5(\not{l}+\not{p}-\not{k}+m_c)\gamma_5(\not{l}+\not{p}+m_d)\gamma_5}{(l^2-m_a^2)((l-p')^2-m_b^2)((l+p-k)^2-m_c^2)((l+p)^2-m_d^2)} + (p\leftrightarrow p',k\leftrightarrow k') + (p\leftrightarrow p') + (k\leftrightarrow k'), \tag{C6}$$

$$I^B_{\phi^4}(p,p',m_a,m_b) = (-1)\int \frac{d^4l}{i(2\pi)^4}\frac{\mathrm{Tr}(\not{l}+m_a)(\not{l}+\not{p}+\not{p}'+m_b)}{(l^2-m_a^2)((l+p+p')^2-m_b^2)}. \tag{C7}$$

At the lowest order in the expansion in the external momenta we obtain

$$I^A_{\phi^4}(0,0,0,0,m_a,m_a,m_c,m_c) = 4I^{1A}_{\phi^4}(m_a,m_c) = -\frac{1}{4\pi^2}\frac{m_a^2\ln(\Lambda^2/m_a^2)-m_c^2\ln(\Lambda^2/m_c^2)}{(m_a^2-m_c^2)}+\cdots, \tag{C8}$$

$$I^A_{\phi^4}(0,0,0,0,m_a,m_a,m_a,m_d) = 4I^{2A}_{\phi^4}(m_a,m_d) = -\frac{1}{4\pi^2}\left(\frac{m_a(m_a^2+m_am_d-m_d^2)\ln(\Lambda^2/m_a^2)-m_d^3\ln(\Lambda^2/m_d^2)}{(m_a-m_d)(m_a+m_d)^2} - \frac{m_a}{m_a+m_d}+\cdots\right), \tag{C9}$$

$$I^A_{\phi^4}(0,0,0,0,m_a,m_a,m_a,m_a) = 4I^{3A}_{\phi^4}(m_a) = -\frac{1}{4\pi^2}(-1+\ln(\Lambda^2/m_a^2)+\cdots), \tag{C10}$$

$$I^B_{\phi^4}(0,0,m_a,m_b) = I^{1B}_{\phi^4}(m_a,m_b) = \frac{-1}{4\pi^2}\left(-\Lambda^2+\frac{m_a^3\ln(\Lambda^2/m_a^2)-m_b^3\ln(\Lambda^2/m_b^2)}{m_a-m_b}+\cdots\right), \tag{C11}$$

$$I^B_{\phi^4}(0,0,m_a,m_a) = I^{2B}_{\phi^4}(m_a) = \frac{-1}{4\pi^2}(-\Lambda^2-2m_a^2+3m_a^2\ln(\Lambda^2/m_a^2)+\cdots), \tag{C12}$$

where $\cdots$ stands for terms of $O(\Lambda^{-2})$ and higher. These expressions are used for the effective couplings defined in (32)–(35).

(vi) ϕ-ϕ-S amplitude

To obtain the $\phi(p)$-$\phi(p')$-$S(k)$ three-point function (Fig. 7) we need

$$I^A_{\phi^2 S}(p,p',m_a,m_b) = (-1)\int \frac{d^4l}{i(2\pi)^4}\frac{\mathrm{Tr}(\not{l}+\not{p}+m_b)\gamma_5(\not{l}+m_a)\gamma_5(\not{l}-\not{p}'+m_b)}{((l+p)^2-m_b^2)(l^2-m_a^2)((l-p')^2-m_b^2)}+(p\leftrightarrow p'), \tag{C13}$$

$$I^B_{\phi^2 S}(p,p',m_a) = (-1)\int \frac{d^4l}{i(2\pi)^4}\frac{\mathrm{Tr}(\not{l}+\not{p}+\not{p}'+m_a)(\not{l}+m_a)}{((l+p+p')^2-m_a^2)(l^2-m_a^2)}. \tag{C14}$$

At the lowest order in the expansion in the external momenta we obtain

$$I^A_{\phi^2 S}(0,0,m_a,m_b) = 2I^{1A}_{\phi^2 S}(m_a,m_b) = \frac{1}{2\pi^2}\left(-\frac{m_b^2}{m_a+m_b}-\frac{1}{2}(m_a-m_b)\ln(\Lambda^2/m_b^2)+\frac{m_a^3}{2(m_a+m_b)^2}\ln(m_a^2/m_b^2)+\cdots\right), \tag{C15}$$

$$I^{A}_{\phi^2 S}(0,0,m_a,m_a) = 2I^{2A}_{\phi^2 S}(m_a) = \frac{m_a}{4\pi^2}(-1+\ln(\Lambda^2/m_a^2)+\cdots), \tag{C16}$$

$$I^{B}_{\phi^2 S}(0,0,m_a) = I^{B}_{\phi^2 S}(m_a) = \frac{1}{4\pi^2}(\Lambda^2+2m_a^2-3m_a^2\ln(\Lambda^2/m_a^2)+\cdots). \tag{C17}$$

These expressions are used for the effective couplings defined in (37)–(39).

(vii) ϕ-ϕ-S-S amplitude

Similarly,

$$I^{A}_{\phi^2 S^2}(p,p',k,k',m_a,m_b,m_c,m_d) = (-1)\int \frac{d^4l}{i(2\pi)^4}\frac{\mathrm{Tr}(\not{l}+m_a)\gamma_5(\not{l}-\not{p}'+m_b)(\not{l}+\not{p}-\not{k}+m_b)(\not{l}+\not{p}+m_b)\gamma_5}{(l^2-m_a^2)((l-p')^2-m_b^2)((l+p-k)^2-m_b^2)((l+p)^2-m_b^2)} + (k\leftrightarrow k'), \tag{C18}$$

$$I^{B}_{\phi^2 S^2}(p,p',k,k',m_a,m_b,m_c,m_d) = (-1)\int \frac{d^4l}{i(2\pi)^4}\frac{\mathrm{Tr}(\not{l}+m_a)(\not{l}+\not{k}'+m_a)\gamma_5(\not{l}+\not{p}-\not{k}+m_b)(\not{l}+\not{p}+m_b)\gamma_5}{(l^2-m_a^2)((l+k')^2-m_b^2)((l+p-k)^2-m_b^2)((l+p)^2-m_b^2)} + (k\leftrightarrow k'), \tag{C19}$$

$$I^{C}_{\phi^4}(p,p',m_a) = (-1)\int \frac{d^4l}{i(2\pi)^4}\frac{\mathrm{Tr}(\not{l}-\not{k}'+m)(\not{l}+m)(\not{l}+\not{k}+m)}{((l+k)^2-m^2)(l^2-m^2)((l-k')^2-m^2)} + (k\leftrightarrow k'). \tag{C20}$$

At the lowest order in the expansion in the external momenta we obtain

$$I^{A}_{\phi^2 S^2}(0,0,0,0,m_a,m_b) = 2I^{1A}_{\phi^2 S^2}(m_a,m_b) = -\frac{1}{2\pi^2}\left[\frac{1}{(m_a+m_b)^2}\left(m_b(5m_a+3m_b)+\frac{m_a^3}{(m_a+m_b)}\ln(m_a^2/m_b^2)\right) - \ln(\Lambda^2/m_a^2)+\cdots\right], \tag{C21}$$

$$I^{A}_{\phi^2 S^2}(0,0,0,0,m_a,m_a) = 2I^{2A}_{\phi^2 S^2}(m_a) = -\frac{1}{2\pi^2}(2-\ln(\Lambda^2/m_a^2)+\cdots), \tag{C22}$$

$$I^{B}_{\phi^2 S^2}(0,0,0,0,m_a,m_b) = 2I^{1B}_{\phi^2 S^2}(m_a,m_b) = -\frac{1}{2\pi^2}\frac{1}{(m_a+m_b)^2}\left(\frac{m_a^2(m_a+3m_b)\ln(\Lambda^2/m_a^2)+m_b^2(m_b+3m_a)\ln(\Lambda^2/m_b^2)}{(m_a+m_b)} - 2(m_a^2+m_b^2)+\cdots\right), \tag{C23}$$

$$I^{B}_{\phi^2 S^2}(0,0,0,0,m_a,m_a) = 2I^{2B}_{\phi^2 S^2}(m_a) = -\frac{1}{2\pi^2}(-1+\ln(\Lambda^2/m_a^2)+\cdots), \tag{C24}$$

$$I^{C}_{\phi^2 S^2}(0,m) = 2I^{C}_{\phi^2 S^2}(m) = \frac{m}{2\pi^2}(5-3\ln(\Lambda^2/m^2)+\cdots). \tag{C25}$$

These expressions are used for the effective couplings defined in (41)–(43).

(viii) ϕ-ϕ-γ-γ amplitude

The next example is the $\phi(p)$-$\phi(p')$-$\gamma(k)$-$\gamma(k')$ four-point function. The diagrams at the one-loop level are shown in Fig. 9:

$$I^{A,\mu\nu}_{0,\phi^2}(p,p',k,k',m_a,m_b,m_c) = (-1)\int \frac{d^4l}{i(2\pi)^4}\frac{\mathrm{Tr}(\not{l}+m_a)\gamma_5(\not{l}-\not{p}'+m_b)\gamma^\mu(\not{l}+\not{p}-\not{k}+m_c)\gamma^\nu(\not{l}+\not{p}+m_b)\gamma_5}{(l^2-m_a^2)((l-p')^2-m_b^2)((l+p-k)^2-m_c^2)((l+p)^2-m_b^2)} + (p\leftrightarrow p',k\leftrightarrow k',\mu\leftrightarrow\nu)+(k\leftrightarrow k',\mu\leftrightarrow\nu)+(p\leftrightarrow p'), \tag{C26}$$

$$I^{B,\mu\nu}_{0,\phi^2}(p,p',k,k',m_a,m_b) = (-1)\int \frac{d^4l}{i(2\pi)^4}\frac{\mathrm{Tr}(\not{l}-\not{k}+m_a)\gamma^\nu(\not{l}+m_a)\gamma_5(\not{l}-\not{p}'+m_b)\gamma^\mu(\not{l}+\not{p}-\not{k}+m_b)\gamma_5}{((l-k)^2-m_a^2)(l^2-m_a^2)((l-p')^2-m_b^2)((l+p-k)^2-m_b^2)} + (p\leftrightarrow p'), \tag{C27}$$

$$I^{C,\mu\nu}_{0,\phi^2}(k,k',m) = (-1)\int \frac{d^4l}{i(2\pi)^4}\frac{\mathrm{Tr}(\not{l}-\not{k}'+m)\gamma^\mu(\not{l}+m)\gamma^\nu(\not{l}+\not{k}+m)}{((l+k)^2-m^2)(l^2-m^2)((l-k')^2-m^2)} + (k\leftrightarrow k',\mu\leftrightarrow\nu). \tag{C28}$$

The subscript 0 indicates that the amplitudes are unsubtracted, and therefore they are not gauge invariant. We apply the least subtraction method to obtain gauge invariant amplitudes $I^{A,\mu\nu}_{\phi^2}, I^{B,\mu\nu}_{\phi^2}$, and $I^{C,\mu\nu}_{\phi^2}$, respectively. Since the realistic parameter space is close to that of the $SU(2)_V$ case (8), we consider them only in this case. At the lowest order in the expansion in the external momenta we obtain

$$I^{A,\mu\nu}_{\phi^2}(k,k',m) + I^{B,\mu\nu}_{\phi^2}(k,k',m) = \frac{1}{6\pi^2m^2}(k\cdot k'g^{\mu\nu}-k^\mu k'^\nu)+\cdots \tag{C29}$$

$$I^{C,\mu\nu}_{\phi^2}(k,k',m) = -\frac{1}{6\pi^2m}(k\cdot k'g^{\mu\nu}-k^\mu k'^\nu)+\cdots \tag{C30}$$

in the large Λ limit. The result is used for the effective Lagrangian (44) and (61).

APPENDIX D: LEAST SUBTRACTION PROCEDURE

The cutoff Λ breaks gauge invariance explicitly and to restore gauge invariance we have to subtract non-gauge invariant terms from the original amplitude. In renormalizable theories there is no problem to define a finite renormalized gauge invariant amplitude. In the limit of $\Lambda\to\infty$ the gauge noninvariant terms are a finite number of local terms, which can be cancelled by the corresponding local counterterms so that the subtracted amplitude is, up to its normalization, independent of the regularization scheme. To achieve such a uniqueness in cutoff theories, one needs an additional prescription.

In [52] a novel method called the "*least subtraction procedure*" has been proposed. The basic idea is to keep the subtraction terms to the minimum necessary. Consider an unsubtracted amplitude

$$\mathcal{A}_{0,\mu_1\ldots\mu_{n_g}}(\Lambda;p_1\ldots p_{n_s},k_1\ldots k_{n_g}), \tag{D1}$$

with n_g photons and n_s scalars (scalars and axial scalars). Expand the amplitude in the external momenta k's and p's:

$$\mathcal{A}_{0,\mu_1\ldots\mu_{n_g}} = \sum_{m=0}\mathcal{A}^{(m)}_{0,\mu_1\ldots\mu_{n_g}}, \tag{D2}$$

where $\mathcal{A}^{(m)}_{0,\mu_1\ldots\mu_{n_g}}$ consists of mth order monomials of the external momenta. In general, $\mathcal{A}^{(0)}_{0,\mu_1\ldots\mu_{n_g}} = \mathcal{A}_{0,\mu_1\ldots\mu_{n_g}}$ at $p=0,k=0$ is nonvanishing and we can subtract it because it is not gauge invariant. We keep the tensor structure of $\mathcal{A}^{(0)}_{0,\mu_1\ldots\mu_{n_g}}$ as the tensor structure of the counterterms for $\mathcal{A}^{(m)}_{0,\mu_1\ldots\mu_{n_g}}(m>0)$ until a new tensor structure for the counterterms is required. We continue this until no more new tensor structure is needed.

To illustrate the subtraction method we consider the $S(p)$-$\gamma(k)$-$\gamma(k')$ three-point function, which is given by

$$\mathcal{A}_{0,\mu\nu}(k,k') = \sum_{i=1}^{3} y_i n_c e^2 Q^2 \int \frac{d^4l}{i(2\pi)^4}\frac{\mathrm{Tr}(\not{l}-\not{k}'+M_i)\gamma_\mu(\not{l}+M_i)\gamma_\nu(\not{l}+\not{k}+M_i)}{((l+k)^2-M_i^2)(l^2-M_i^2)((l-k')^2-M_i^2)} + (k\leftrightarrow k',\mu\leftrightarrow\nu), \tag{D3}$$

where we use the on shell conditions $k^2=k'^2=0$. Without loss of generality the amplitude can be written as

$$\mathcal{A}_{0,\mu\nu}(k,k') = \mathcal{A}_{0,g}(k,k')g_{\mu\nu} + \mathcal{A}_{0,k}(k,k')k_\mu k'_\nu + \mathcal{B}_{0,k}(k,k')k_\nu k'_\mu. \tag{D4}$$

The last term does not contribute to the gauge invariance $k^\nu\mathcal{A}_{\mu\nu}(k,k') = k'^\mu\mathcal{A}_{\mu\nu}(k,k') = 0$, and so we ignore it. The corresponding one-loop diagram is the one in Fig. 4 with $\tilde{\eta}$ replaced by S. According to the least subtraction method, we expand the amplitude in the external momenta k and k'. At the second order, for instance, we find

$$\mathcal{A}^{(2)}_{0,g}(k,k') = -\frac{n_c e^2 Q^2}{4\pi^2}(k\cdot k') \times \sum_i \frac{y_i \Lambda^4}{3M_i(\Lambda^2+M_i^2)^3}(2\Lambda^2+M_i^2), \quad \text{(D5)}$$

$$\mathcal{A}^{(2)}_{0,k}(k,k') = \frac{n_c e^2 Q^2}{4\pi^2}\sum_i \frac{y_i \Lambda^4}{3M_i(\Lambda^2+M_i^2)^3}(2\Lambda^2+2M_i^2). \quad \text{(D6)}$$

In the $\Lambda \to \infty$ limit the second order amplitude will be gauge invariant, but it is not at a finite Λ. Moreover, there are infinitely many ways of subtraction to make the second order amplitude gauge invariant. However, none of them is preferential. The least subtraction method uses the lower order amplitude, i.e.,

$$\mathcal{A}^{(0)}_{0,g}(k,k') = -\sum_i \frac{\Lambda^4 M_i}{(\Lambda^2+M_i^2)^2}, \qquad \mathcal{A}^{(0)}_{0,k}(k,k') = 0 \quad \text{(D7)}$$

in this case, how to subtract the second order amplitude. At the lowest order in the derivative expansion, what is to be subtracted is unique; it is the $g_{\mu\nu}$ term. We keep this tensor structure as the tensor structure of the counterterms for higher order terms until a new tensor structure for the counterterms is required. However, in the case of $\mathcal{A}_{0,\mu\nu}(k,k')$ there will be no new tensor structure appearing in higher orders. This implies that $\mathcal{A}_{0,k}(k,k')$ remains unsubtracted [i.e., $\mathcal{A}_k(k,k') = \mathcal{A}_{0,k}(k,k')$] so that the subtracted gauge invariant amplitude is given by

$$\begin{aligned}\mathcal{A}_{\mu\nu}(k,k') &= -\sum_i \frac{y_i n_c e^2 Q^2}{4\pi^2}(g_{\mu\nu}k\cdot k' - k_\mu k'_\nu)\left(\frac{\Lambda^4}{M_i(\Lambda^2+M_i^2)^2}\right) \\ &\quad\times\left[\frac{2}{3}+\frac{7k\cdot k'(\Lambda^2+3M_i^2)}{90M_i^2(\Lambda^2+M_i^2)}+\frac{(k\cdot k')^2(\Lambda^4+4\Lambda^2M_i^2+6M_i^4)}{63M_i^4(\Lambda^2+M_i^2)^2}+\cdots\right] \\ &= -\sum_i \frac{y_i n_c e^2 Q^2 M_i}{4\pi^2}(g_{\mu\nu}k\cdot k' - k_\mu k'_\nu)\int_0^1 dx\int_0^{1-x} dy\,\frac{2\Lambda^4}{(\Lambda^2+D^2)^2}\frac{(1-4xy)}{D^2}, \end{aligned} \quad \text{(D8)}$$

where $D = M_i^2 - 2xyk\cdot k'$.

[1] F. Wilczek, Mass without mass I: Most of matter, Phys. Today **52**, 11–13 (1999).

[2] G. Aad *et al.* (ATLAS Collaboration), Observation of a new particle in the search for the standard model Higgs boson with the ATLAS detector at the LHC, Phys. Lett. B **716**, 1 (2012).

[3] S. Chatrchyan *et al.* (CMS Collaboration), Observation of a new boson at a mass of 125 GeV with the CMS experiment at the LHC, Phys. Lett. B **716**, 30 (2012).

[4] K. A. Olive *et al.* (Particle Data Group Collaboration), Review of particle physics, Chin. Phys. C **38**, 090001 (2014).

[5] M. Holthausen, K. S. Lim, and M. Lindner, Planck scale boundary conditions and the Higgs mass, J. High Energy Phys. 02 (2012) 037.

[6] G. Degrassi, S. Di Vita, J. Elias-Miro, J. R. Espinosa, G. F. Giudice, G. Isidori, and A. Strumia, Higgs mass and vacuum stability in the Standard Model at NNLO, J. High Energy Phys. 08 (2012) 098; D. Buttazzo, G. Degrassi, P. P. Giardino, G. F. Giudice, F. Sala, A. Salvio, and A. Strumia, Investigating the near-criticality of the Higgs boson, J. High Energy Phys. 12 (2013) 089.

[7] F. Bezrukov, M. Y. Kalmykov, B. A. Kniehl, and M. Shaposhnikov, Higgs boson mass and new physics, J. High Energy Phys. 10 (2012) 140.

[8] W. A. Bardeen, Report No. FERMILAB-CONF-95-391-T.

[9] C. G. Callan, Jr., Broken scale invariance in scalar field theory, Phys. Rev. D **2**, 1541 (1970); K. Symanzik, Small distance behavior in field theory and power counting, Commun. Math. Phys. **18**, 227 (1970).

[10] S. R. Coleman and E. J. Weinberg, Radiative corrections as the origin of spontaneous symmetry breaking, Phys. Rev. D **7**, 1888 (1973).

[11] J. P. Fatelo, J. M. Gerard, T. Hambye, and J. Weyers, Symmetry Breaking Induced by Top Loops, Phys. Rev. Lett. **74**, 492 (1995).

[12] R. Hempfling, The next-to-minimal Coleman-Weinberg model, Phys. Lett. B **379**, 153 (1996).

[13] T. Hambye, Symmetry breaking induced by top quark loops from a model without scalar mass, Phys. Lett. B **371**, 87 (1996).

[14] K. A. Meissner and H. Nicolai, Conformal symmetry and the standard model, Phys. Lett. B **648**, 312 (2007); Effective action, conformal anomaly and the issue of quadratic

divergences, Phys. Lett. B **660**, 260 (2008); Conformal invariance from non-conformal gravity, Phys. Rev. D **80**, 086005 (2009).

[15] R. Foot, A. Kobakhidze, and R. R. Volkas, Electroweak Higgs as a pseudo-Goldstone boson of broken scale invariance, Phys. Lett. B **655**, 156 (2007); Cosmological constant in scale-invariant theories, Phys. Rev. D **84**, 075010 (2011).

[16] R. Foot, A. Kobakhidze, K. L. McDonald, and R. R. Volkas, Neutrino mass in radiatively-broken scale-invariant models, Phys. Rev. D **76**, 075014 (2007); A solution to the hierarchy problem from an almost decoupled hidden sector within a classically scale invariant theory, Phys. Rev. D **77**. 035006 (2008); Poincar00E9 protection for a natural electroweak scale, Phys. Rev. D **89**, 115018 (2014).

[17] W.-F. Chang, J. N. Ng, and J. M. S. Wu, Shadow Higgs from a scale-invariant hidden U(1)(s) model, Phys. Rev. D **75**, 115016 (2007).

[18] T. Hambye and M. H. G. Tytgat, Electroweak symmetry breaking induced by dark matter, Phys. Lett. B **659**, 651 (2008).

[19] S. Iso, N. Okada, and Y. Orikasa, Classically conformal B^- L extended standard model, Phys. Lett. B **676**, 81 (2009); The minimal B-L model naturally realized at TeV scale, Phys. Rev. D **80**, 115007 (2009); S. Iso and Y. Orikasa, TeV Scale B-L model with a flat Higgs potential at the Planck scale—in view of the hierarchy problem, Prog. Theor. Exp. Phys. **2013**, 023B08 (2013).

[20] M. Holthausen, M. Lindner, and M. A. Schmidt, Radiative symmetry breaking of the minimal left-right symmetric model, Phys. Rev. D **82**, 055002 (2010).

[21] K. Ishiwata, Dark matter in classically scale-invariant two singlets standard model, Phys. Lett. B **710**, 134 (2012).

[22] C. Englert, J. Jaeckel, V. V. Khoze, and M. Spannowsky, Emergence of the electroweak scale through the Higgs portal, J. High Energy Phys. 04 (2013) 060.

[23] V. V. Khoze and G. Ro, Leptogenesis and neutrino oscillations in the classically conformal standard model with the Higgs portal, J. High Energy Phys. 10 (2013) 075.

[24] C. D. Carone and R. Ramos, Classical scale-invariance, the electroweak scale and vector dark matter, Phys. Rev. D **88**, 055020 (2013).

[25] A. Farzinnia, H.-J. He, and J. Ren, Natural electroweak symmetry breaking from scale invariant Higgs mechanism, Phys. Lett. B **727**, 141 (2013).

[26] F. Gretsch and A. Monin, Dilaton: Saving conformal symmetry, arXiv:1308.3863.

[27] Y. Kawamura, Naturalness, conformal symmetry and duality, Prog. Theor. Exp. Phys. **2013** (2013) 113B04.

[28] V. V. Khoze, Inflation and dark matter in the Higgs portal of classically scale invariant standard model, J. High Energy Phys. 11 (2013) 215.

[29] E. Gabrielli, M. Heikinheimo, K. Kannike, A. Racioppi, M. Raidal, and C. Spethmann, Towards completing the standard model: Vacuum stability, EWSB and dark matter, Phys. Rev. D **89**, 015017 (2014).

[30] S. Abel and A. Mariotti, Novel Higgs potentials from gauge mediation of exact scale breaking, Phys. Rev. D **89**, 125018 (2014).

[31] M. Ibe, S. Matsumoto, and T. T. Yanagida, Flat Higgs potential from Planck scale supersymmetry breaking, Phys. Lett. B **732**, 214 (2014).

[32] C. T. Hill, Is the Higgs boson associated with Coleman-Weinberg dynamical symmetry breaking?, Phys. Rev. D **89**, 073003 (2014).

[33] J. Guo and Z. Kang, Higgs naturalness and dark matter stability by scale invariance, arXiv:1401.5609.

[34] S. Benic and B. Radovcic, Electroweak breaking and dark matter from the common scale, Phys. Lett. B **732** 91 (2014); Majorana dark matter in a classically scale invariant model, J. High Energy Phys. 01 (2015) 143.

[35] V. V. Khoze, C. McCabe, and G. Ro, Higgs vacuum stability from the dark matter portal, J. High Energy Phys. 08 (2014) 026.

[36] H. Davoudiasl and I. M. Lewis, Right-handed neutrinos as the origin of the electroweak scale, Phys. Rev. D **90**, 033003 (2014).

[37] P. H. Chankowski, A. Lewandowski, K. A. Meissner, and H. Nicolai, Softly broken conformal symmetry and the stability of the electroweak scale, Mod. Phys. Lett. A **30**, 1550006 (2015).

[38] K. Allison, C. T. Hill, and G. G. Ross, Ultra-weak sector, Higgs boson mass, and the dilaton, Phys. Lett. B **738**, 191 (2014); An ultra-weak sector, the strong ***CP*** problem and the pseudo-Goldstone dilaton, Nucl. Phys. **B891**, 613 (2015).

[39] A. Farzinnia and J. Ren, Higgs partner searches and dark matter phenomenology in a classically scale invariant Higgs boson sector, Phys. Rev. D **90**, 015019 (2014).

[40] P. Ko and Y. Tang, Galactic center γ-ray excess in hidden sector DM models with dark gauge symmetries: Local Z_3 symmetry as an example, J. Cosmol. Astropart. Phys. 01 (2015) 023.

[41] W. Altmannshofer, W. A. Bardeen, M. Bauer, M. Carena, and J. D. Lykken, Light dark matter, naturalness, and the radiative origin of the electroweak scale, J. High Energy Phys. 01 (2015) 032.

[42] Z. Kang, FImP miracle of sterile neutrino dark matter by scale invariance, arXiv:1411.2773.

[43] G. F. Giudice, G. Isidori, A. Salvio, and A. Strumia, Softened gravity and the extension of the standard model up to infinite energy, J. High Energy Phys. 02 (2015) 137.

[44] J. Guo, Z. Kang, P. Ko, and Y. Orikasa, Accidental dark matter: Case in the scale invariant local $B-L$ models, arXiv:1502.00508.

[45] K. Kannike, G. Hütsi, L. Pizza, A. Racioppi, M. Raidal, A. Salvio, and A. Strumia, Dynamically induced Planck scale and inflation, arXiv:1502.01334.

[46] Y. Nambu, Axial Vector Current Conservation in Weak Interactions, Phys. Rev. Lett. **4**, 380 (1960).

[47] Y. Nambu and G. Jona-Lasinio, Dynamical model of elementary particles based on an analogy with superconductivity. 1., Phys. Rev. **122**, 345 (1961); Dynamical model of elementary particles based on an analogy with superconductivity. Ii, Phys. Rev. **124**, 246 (1961).

[48] T. Hur, D.-W. Jung, P. Ko, and J. Y. Lee, Electroweak symmetry breaking and cold dark matter from strongly interacting hidden sector, Phys. Lett. B **696**, 262 (2011).

[49] T. Hur and P. Ko, Scale Invariant Extension of the Standard Model with Strongly Interacting Hidden Sector, Phys. Rev. Lett. **106**, 141802 (2011).

[50] M. Heikinheimo, A. Racioppi, M. Raidal, C. Spethmann, and K. Tuominen, Physical naturalness and dynamical breaking of classical scale invariance, Mod. Phys. Lett. A **29**, 1450077 (2014).

[51] M. Holthausen, J. Kubo, K. S. Lim, and M. Lindner, Electroweak and conformal symmetry breaking by a strongly coupled hidden sector, J. High Energy Phys. 12 (2013) 076.

[52] J. Kubo, K. S. Lim, and M. Lindner, Gamma-ray line from Nambu-Goldstone dark matter in a scale invariant extension of the standard model, J. High Energy Phys. 09 (2014) 016.

[53] O. Antipin, M. Redi, and A. Strumia, Dynamical generation of the weak and dark matter scales from strong interactions, J. High Energy Phys. 01 (2015) 157.

[54] M. Heikinheimo and C. Spethmann, Galactic centre GeV photons from dark technicolor, J. High Energy Phys. 12 (2014) 084.

[55] S. Weinberg, Implications of dynamical symmetry breaking, Phys. Rev. D **13**, 974 (1976); Implications of dynamical symmetry breaking: An addendum, Phys. Rev. D **19**, 1277 (1979).

[56] L. Susskind, Dynamics of spontaneous symmetry breaking in the Weinberg-Salam theory, Phys. Rev. D **20**, 2619 (1979).

[57] J. Kubo, K. S. Lim, and M. Lindner, Electroweak Symmetry Breaking via QCD, Phys. Rev. Lett. **113**, 091604 (2014).

[58] T. Hatsuda and T. Kunihiro, QCD phenomenology based on a chiral effective Lagrangian, Phys. Rep. **247**, 221 (1994).

[59] T. Kunihiro and T. Hatsuda, A self-consistent mean field approach to the dynamical symmetry breaking: The effective potential of the Nambu-Jona-Lasinio model, Prog. Theor. Phys. **71**, 1332 (1984); Fluctuation Effects in Hot Quark Matter: Precursors of Chiral Transition at Finite Temperature, Phys. Rev. Lett. **55**, 158 (1985); Effects of flavor mixing induced by axial anomaly on the quark condensates and meson spectra, Phys. Lett. B **206**, 385 (1988); **210**, 278(E) (1988).

[60] M. J. Strassler and K. M. Zurek, Echoes of a hidden valley at hadron colliders, Phys. Lett. B **651**, 374 (2007); T. Han, Z. Si, K. M. Zurek, and M. J. Strassler, Phenomenology of hidden valleys at hadron colliders, J. High Energy Phys. 07 (2008) 008.

[61] J. H. Lowenstein and W. Zimmermann, Infrared convergence of Feynman integrals for the massless a**4 model, Commun. Math. Phys. **46**, 105 (1976); The power counting theorem for Feynman integrals with massless propagators, Commun. Math. Phys. **44**, 73 (1975); The power counting theorem for Feynman integrals with massless propagators, Lect. Notes Phys. **558**, 310 (2000).

[62] E. C. Poggio and H. R. Quinn, The infrared behavior of zero-mass Green's functions and the absence of quark confinement in perturbation theory, Phys. Rev. D **14**, 578 (1976).

[63] E. Witten, Cosmic separation of phases, Phys. Rev. D **30**, 272 (1984).

[64] C. J. Hogan, Gravitational radiation from cosmological phase transitions, Mon. Not. R. Astron. Soc. **218**, 629 (1986).

[65] P. Amaro-Seoane, S. Aoudia, S. Babak, P. Binetruy, E. Berti, A. Bohe, C. Caprini, M. Colpi *et al.*, eLISA/NGO: Astrophysics and cosmology in the gravitational-wave millihertz regime, GW Notes **6**, 4 (2013); P. Schwaller, Gravitational waves from a dark (twin) phase transition, arXiv:1504.07263.

[66] M. Aoki, M. Duerr, J. Kubo, and H. Takano, Multi-component dark matter systems and their observation prospects, Phys. Rev. D **86**, 076015 (2012).

[67] S. Tulin, H. B. Yu, and K. M. Zurek, Three exceptions for thermal dark matter with enhanced annihilation to $\gamma\gamma$, Phys. Rev. D **87**, 036011 (2013); S. Baek, P. Ko, and E. Senaha, Can Zee-Babu model implemented with scalar dark matter explain both Fermi/LAT 130 GeV γ-ray excess and neutrino physics?, J. High Energy Phys. 09 (2014) 153; M. Aoki, J. Kubo, and H. Takano, Two-loop radiative seesaw mechanism with multicomponent dark matter explaining the possible excess in the Higgs boson decay and at the Fermi LAT, Phys. Rev. D **87**, 116001 (2013).

[68] M. Ackermann *et al.* (LAT Collaboration), Fermi LAT search for dark matter in gamma-ray lines and the inclusive photon spectrum, Phys. Rev. D **86**, 022002 (2012).

[69] M. Gustafsson (for the Fermi-LAT Collaboration), Fermi-LAT and the gamma-ray line search, arXiv:1310.2953.

[70] A. Abramowski *et al.* (H.E.S.S. Collaboration), Search for Photon Line-like Signatures from Dark Matter Annihilations with H.E.S.S, Phys. Rev. Lett. **110**, 041301 (2013).

[71] P. A. R. Ade *et al.* (Planck Collaboration), Planck 2015 results. XIII. Cosmological parameters, arXiv:1502.01589.

[72] T. Bringmann, L. Bergstrom, and J. Edsjo, New gamma-ray contributions to supersymmetric dark matter annihilation, J. High Energy Phys. 01 (2008) 049.

[73] G. Bertone, C. B. Jackson, G. Shaughnessy, T. M. P. Tait, and A. Vallinotto, The WIMP forest: Indirect detection of a chiral square, Phys. Rev. D **80**, 023512 (2009).

[74] R. Laha, K. C. Y. Ng, B. Dasgupta, and S. Horiuchi, Galactic Center radio constraints on gamma-ray lines from dark matter annihilation, Phys. Rev. D **87**, 043516 (2013).

[75] R. Barbieri, L. J. Hall, and V. S. Rychkov, Improved naturalness with a heavy Higgs: An alternative road to LHC physics, Phys. Rev. D **74**, 015007 (2006).

[76] J. R. Ellis, A. Ferstl, and K. A. Olive, Reevaluation of the elastic scattering of supersymmetric dark matter, Phys. Lett. B **481**, 304 (2000).

[77] E. Aprile (XENON1T Collaboration), The XENON1T dark matter search experiment, Springer Proc. Phys. **148**, 93 (2013).

[78] K. Kohri and T. Takahashi, Cosmology with long-lived charged massive particles, Phys. Lett. B **682**, 337 (2010).

[79] M. Pospelov, Particle Physics Catalysis of Thermal Big Bang Nucleosynthesis, Phys. Rev. Lett. **98**, 231301 (2007); C. Bird, K. Koopmans, and M. Pospelov, Primordial lithium abundance in catalyzed big bang nucleosynthesis, Phys. Rev. D **78**, 083010 (2008).

[80] M. Pospelov, J. Pradler, and F. D. Steffen, Constraints on supersymmetric models from catalytic primordial

nucleosynthesis of beryllium, J. Cosmol. Astropart. Phys. 11 (2008) 020.

[81] K. Hamaguchi, T. Hatsuda, M. Kamimura, Y. Kino, and T. T. Yanagida, Stau-catalyzed ^{6}Li production in big-bang nucleosynthesis, Phys. Lett. B **650**, 268 (2007); M. Kawasaki, K. Kohri, and T. Moroi, Big-bang nucleosynthesis with long-lived charged slepton, Phys. Lett. B **649**, 436 (2007); M. Kawasaki, K. Kohri, T. Moroi, and A. Yotsuyanagi, Big-bang nucleosynthesis and gravitino, Phys. Rev. D **78**, 065011 (2008).

[82] A. D. Dolgov, S. L. Dubovsky, G. I. Rubtsov, and I. I. Tkachev, Constraints on millicharged particles from Planck data, Phys. Rev. D **88**, 117701 (2013).

[83] P. Langacker and G. Steigman, Requiem for an FCHAMP? Fractionally CHArged, Massive Particle, Phys. Rev. D **84**, 065040 (2011).

[84] J. A. Wheeler, *Geometrodynamics* (Academic Press, New York, 1962).

[85] K. Fujii, in 2nd Toyama International Workshop on Higgs as a Probe of New Physics 2015, http://www3.u-toyama.ac.jp/theory/HPNP2015/Slides/HPNP2015Feb11/Fujii_20150211.pdf.

[86] T. Inagaki, D. Kimura, H. Kohyama, and A. Kvinikhidze, Regularization parameter independent analysis in Nambu-Jona-Lasinio model, Int. J. Mod. Phys. A **28**, 1350164 (2013).